

TESTS OF THE GRAVITATIONAL INVERSE-SQUARE LAW

E.G. Adelberger, B.R. Heckel, and A.E. Nelson

Department of Physics, University of Washington, Seattle, Washington 98195-1560

KEYWORDS: gravitation, experimental tests of inverse-square law, quantum gravity, extra dimensions

ABSTRACT: We review recent experimental tests of the gravitational inverse-square law, and the wide variety of theoretical considerations that suggest the law may break down in experimentally accessible regions.

CONTENTS

INTRODUCTION	2
<i>Background</i>	2
<i>Scope of this review</i>	6
THEORETICAL SPECULATIONS	6
<i>Unifying gravity with particle physics: 2 hierarchy problems</i>	6
<i>Extra dimensions and TeV scale unification of gravity</i>	12
<i>Infinite-volume extra dimensions</i>	19
<i>Exchange forces from conjectured new bosons</i>	21
<i>Attempts to solve the cosmological constant problem</i>	27

EXPERIMENTAL CHALLENGES 30

Signals 30

Noise considerations 32

Backgrounds 33

Experimental strategies 38

EXPERIMENTAL RESULTS 39

Low-frequency torsion oscillators 39

High-frequency torsion oscillators 44

Micro-cantilevers 46

Casimir force experiments 48

Astronomical tests 53

CONCLUSIONS 55

Summary of experimental results 55

Prospects for improvements 55

What if a violation of the $1/r^2$ law were observed? 59

ACKNOWLEDGMENTS 59

NUMBERED LITERATURE CITED 60

1 INTRODUCTION

1.1 Background

Gravitation was the first of the 4 known fundamental interactions to be understood quantitatively and the first “grand unification” in physics; Isaac Newton’s Theory of Universal Gravitation connected terrestrial phenomena (the “falling apple”) with astronomical observations (the “falling Moon” and Kepler’s Laws). This theory stood virtually unchallenged until Albert Einstein developed his rel-

ativistic theory of gravitation in 1917. Since then General Relativity has successfully passed all experimental tests and is today the Standard Model of gravitation. Yet some three centuries after Newton, gravitation remains one of the most puzzling topics in physics. Recently a completely unexpected and fundamentally new gravitational property was discovered using distant Type Ia supernovae: the apparent **acceleration** of the Hubble expansion(1, 2) that is as yet unexplained. Furthermore, gravitation is not included, and in fact not **includable**, in the imposing quantum field theory that constitutes the Standard Model of particle physics. There is a broad consensus that the two Standard Models are incompatible: the strong, weak and electromagnetic interactions are explained as results of the quantum exchange of virtual bosons, while the gravitational interaction is explained as a classical consequence of matter and energy curving space-time. Because quantum field theories cannot describe gravitation and General Relativity predicts an infinite space-time curvature at the center of a black hole, neither of these two standard models is likely to be truly fundamental.

Connecting gravity with the rest of physics is clearly the central challenge of fundamental physics, and for the first time we have a candidate theory (string or M-theory) that may unify gravitation with particle physics. But outstanding theoretical problems remain that have focused attention on possible new phenomena that could show up as deviations from familiar inverse-square law (ISL) of gravity, generally at length scales less than a few millimeters, but sometimes also at astronomical or even cosmological distances. We review these speculations in Section 2.

While it is conventionally assumed that the ISL should be valid for separations from infinity to roughly the Planck length ($R_P = \sqrt{G\hbar/c^3} = 1.6 \times 10^{-35}$ m) it

had, until a few years ago, only been precisely tested for separations ranging from the scale of the solar system down to a few millimeters. The reasons for this are obvious: on the one hand there are no independently known mass distributions on length scales larger than the solar system, and on the other hand, it is difficult to get enough matter in close enough proximity to obtain a background-free gravitational signal at length scales smaller than 1 mm. This contrasts strongly with Coulomb's Law (and its electroweak generalization) which has been tested for separations down to 10^{-18} m in e^+e^- leptonic interactions at high-energy colliders(3). Although Coulomb's Law has not been experimentally verified at length scales large compared to laboratory dimensions, a null-type laboratory measurement looking for effects of the galactic electromagnetic vector potential, A , rules out deviations due a finite photon mass for length scales up to $\sim 2 \times 10^{10}$ m (4).

1.1.1 Parameterizations

Historically, experimental tests of Coulomb's and Newton's inverse-square laws were used to set limits on violations that, for gravity, took the form

$$F(r) = G \frac{m_1 m_2}{r^{2+\epsilon}} . \quad (1)$$

From the perspective of Gauss's Law the exponent 2 is a purely geometrical effect of 3 space dimensions, so that this parameterization was not well-motivated theoretically. Instead, it is now customary to interpret tests of the ISL as setting limits on an additional Yukawa contribution to the familiar $1/r^2$ contribution, which in the gravitational case creates a potential

$$V(r) = -G \frac{m_1 m_2}{r} \left[1 + \alpha e^{-r/\lambda} \right] , \quad (2)$$

where α is a dimensionless strength parameter and λ is a length scale or range. The Yukawa contribution is the static limit of an interaction due the exchange of virtual bosons of mass $m_b = \hbar/(\lambda c)$, where m_b is the boson mass; the Yukawa form is also useful in other contexts (see Sec. 2.2.1 below).

Some investigators (see for example Ref. (5)) have considered the possibility that a non-zero graviton mass could lead to a “pure Yukawa” gravitational potential $V(r) = -Gm_1m_2e^{-r/\lambda}/r$, recognizing that this phenomenological form does not have a well-defined theoretical foundation. Others have considered power law modifications to the ISL(6):

$$V(r) = -G\frac{m_1 m_2}{r} \left[1 + \alpha_N \left(\frac{r_0}{r} \right)^{N-1} \right], \quad (3)$$

where α_N is a dimensionless constant and r_0 corresponds to a new length scale associated with a non-Newtonian process.

Terms with $N = 2$ and $N = 3$ may be generated by the simultaneous exchange of two massless scalar and two massless pseudoscalar particles, respectively(7, 8, 9), while $N = 5$ may be generated by the simultaneous exchange of two massless axions(10) or a massless neutrino-antineutrino pair(11).

In this review, we focus on the parametrization of Eq. 2; any experiment that detects a violation of the ISL will indicate a strength, α , and a length scale, λ , that characterizes the violation. Once a violation is detected, it will become necessary to determine the functional form of the violation. The parameterization of Eq. 2 has strong implications for experimental tests of the ISL. Any one test of the law necessarily covers a limited range of length scales. Suppose, for example, one performs a Keplerian test, comparing the orbits of two planets orbiting a common sun. Clearly, the test is insensitive to λ 's much less than the orbit radius of the inner planet. It is also insensitive to λ 's much larger than the

orbit radius of the outer planet because both planets simply feel a renormalized Newtonian constant $\tilde{G} = G(1 + \alpha)$. Consequently a great variety of experiments are needed to effectively explore a wide variety of length scales. This contrasts with limits on Yukawa interactions from “Equivalence Principle” tests where a single experimental result for a composition-dependent acceleration difference typically provides a constraint on α for λ 's ranging from the length scale of the attractor to infinity (see, for example, Ref. (12)).

1.2 Scope of this review

This review concentrates on experimental tests of the ISL at length scales of millimeters or less, and on the wide range of theoretical developments suggesting that new phenomena may occur in this regime. We also discuss speculations about possible ISL violations at much larger length scales that could have important cosmological implications. A extensive review of experimental results at longer length scales(13) appeared in 1999 which we update in Sec. 4.5 below. A review of extra “gravitational” dimensions, with emphasis on collider signatures, has recently appeared in this review series(14). Our review is focused on work done since 1995, and should be current as of January 2003. An earlier review(12) covered spin-dependent forces that we do not consider here.

2 THEORETICAL SPECULATIONS

2.1 Unifying gravity with particle physics: 2 hierarchy problems

The two greatest triumphs of 20th century physics are General Relativity (GR), and Quantum Mechanics. However we do not currently know how to link these two theories, or how to do calculations consistently in situations where both grav-

ity and quantum effects are important such as for conditions near the Big Bang and the cores of black holes. Clearly General Relativity must be contained in a more fundamental quantum theory that would allow sensible calculations even in extreme conditions. However attempts to quantize General Relativity have been plagued with difficulties. Although one can construct an effective quantum field theory of gravity and particle physics that is sufficiently accurate for many applications, the theory is infamously “nonrenormalizable” or nonpredictive— an infinite number of free parameters are needed to describe quantum effects at arbitrarily short distances to arbitrary precision.

All known nongravitational physics is includable within The Standard Model of particle physics— a quantum field theory in which the weak and electromagnetic interactions are unified into a single framework known as the electroweak theory. Symmetry between the weak and electromagnetic interactions is manifest above a scale of roughly 100 GeV. This unification scale, where the electroweak symmetry is spontaneously broken, is known as the electroweak scale. The electroweak scale is set by a condensate of a scalar field known as the Higgs field that has negative mass-squared term of order $(100 \text{ GeV})^2$ in its potential. All three forces of the Standard Model, the electromagnetic, weak and strong interactions, are similarly unifiable into a simple group with a single coupling at the fantastically high energy scale of 10^{16} GeV. This “grand” unified theory (GUT) successfully explains the quantization of electric charge and, provided there exists a new symmetry between fermions and bosons known as supersymmetry, predicts the observed value for the relative strengths of the weak and electromagnetic couplings. But supersymmetry has not yet been observed in nature and, if present, must be spontaneously broken. Supersymmetry and grand unified theories have been

reviewed in Refs. (15, 16, 17, 18, 19, 20, 21, 22, 23, 24, 25, 26).

Intriguingly, the Planck scale, $M_P = \sqrt{\hbar c/G}$, at which quantum-gravity effects must become important, $M_P c^2 = 1.2 \times 10^{19}$ GeV, is rather close to the apparent unification scale of the other forces. This hints that all belong together in a unified framework, containing a fundamental scale of order M_P . Motivated by GUTs, the conventional view is that the phenomenal weakness of gravity at accessible energies— 10^{32} times weaker than the other forces at the electroweak scale—is due to the small masses of observed particles relative to M_P .

In the Standard Model, particle masses derive from the Higgs condensate. The tremendous discrepancy between the scale of this condensate and the presumed fundamental scale of physics is known as the **gauge hierarchy problem**. In the minimal Standard Model, the smallness of the Higgs mass-squared parameter relative to the GUT or Planck scales violates a principle known as “naturalness” — renormalized values of parameters that receive large quantum corrections should not be much smaller than the size of the corrections. The Higgs mass-squared receives corrections proportional to the cutoff, or maximum scale of validity of the theory. Naturalness would therefore demand that to describe physics at energies higher than about a TeV, the Standard Model should be contained within a more fundamental theory, in which the quantum corrections to the Higgs mass are suppressed. An example of such a theory is a supersymmetric extension of the standard model. In theories with (spontaneously or softly broken) supersymmetry, the quantum corrections to scalar masses are proportional to the supersymmetry-breaking scale. Provided the supersymmetry-breaking scale is of order 100 GeV, the electroweak scale is natural, and the hierarchy question is why the supersymmetry-breaking scale is so small compared to M_P . This latter

problem is theoretically tractable; in many supersymmetric models the scale of supersymmetry breaking is proportional to exponentially small, nonperturbative quantum effects (27, 28).

A second, and much bigger, hierarchy problem is known as the **cosmological constant problem**. The strong observational evidence (1, 2) that the expansion of the universe is accelerating can be explained by a nonvanishing cosmological constant. The concordance of cosmological data indicates(29) that the universe is filled with a vacuum-energy density $\rho_{\text{vac}} \sim 0.7\rho_c$ where ρ_c is the critical density $3H^2c^2/(8\pi G)$ and H is the present value of the Hubble constant. This gives $\rho_{\text{vac}} \sim 4 \text{ keV/cm}^3$ which corresponds to an energy scale $\sqrt[4]{(\hbar c)^3 \rho_{\text{vac}}} \approx 2 \text{ meV}$ or a length scale $\sqrt[4]{(\hbar c)/\rho_{\text{vac}}} \sim 100 \mu\text{m}$. Such a small energy density is particularly puzzling because the quantum corrections to the vacuum energy density from particle physics scale as the fourth power of the cutoff of the effective theory. Such a cutoff might be provided by new physics in the gravitational sector. The energy scale of new gravitational physics has been presumed to be around M_P , which would imply a cosmological constant 10^{120} times larger than observed. The success of the particle physics Standard Model at collider energy scales is inconsistent with a cutoff lower than a TeV. Even a relatively low TeV cutoff gives a theoretical contribution to the cosmological constant that is 10^{60} times larger than experiment. Refs. (30, 31) conjecture that this monstrous discrepancy could be eliminated with a much lower cutoff for the gravitational sector of the effective theory, around an meV, corresponding to new gravitational physics at a distance of about a hundred microns. The theoretical framework for such a low gravity scale is necessarily very speculative. However, just as the gauge hierarchy compels experimental exploration of the TeV scale, the cosmological-constant

problem strongly motivates sub-millimeter scale tests of gravity.

General Relativity itself gives indications that the theory of quantum gravity is radically different from a conventional quantum field theory. For instance, it is known that in theories of gravity, the concept of entropy must be generalized because entropy cannot be an extensive quantity scaling like volume. In fact there is strong evidence in favor of an upper bound on the entropy of any region that scales as the surface area of the boundary of the region (32, 33, 34). A further conjecture, the “holographic principle”, suggests that this entropy bound indicates that the fundamental degrees of freedom of a gravitational theory can actually be formulated in a lower-dimensional theory. Ref. (35) gives a nice review of these ideas and their subsequent development.

M-theory is a popular candidate for a theory of quantum gravity. This theory was called string theory when it was believed that its fundamental degrees of freedom were 1-dimensional objects propagating in a 10-dimensional space-time. Six of these dimensions were assumed to be rolled up into a compact manifold of size $\sim R_P$ and unobservable. We now know that “string” theory necessarily contains many types of objects, known as “branes” or “p-branes”, where p, the number of spatial dimensions of the p-brane, can be anywhere from 0 to 9. This realization has revolutionized our understanding of string theory. Furthermore, string theory is “dual”, or physically equivalent as a quantum theory, to an 11-dimensional theory known as M-theory. There is much theoretical evidence that all known consistent string theories, as well as 11-dimensional supergravity, are just weakly-coupled limits in different vacua of a **single** theory of quantum gravity.

Extra dimensions might seem to be in conflict with the holographic assertion

that the fundamental theory is actually **lower** dimensional. However, as comprehensively reviewed in (36), the discovery that string theory on certain space-times with n non-compact dimensions is dual to a non-gravitational gauge theory with $n - 1$ dimensions provides additional theoretical evidence for holography, as well as for string theory. Strings, M-theory, p-branes, and duality have been reviewed in Refs. (37, 40, 41, 42, 43, 44, 45, 46, 47, 48, 49, 50, 51, 52, 53) and are the subject of several excellent textbooks(38, 39).

Until recently, it was believed that experimental verification of a theory of quantum gravity was out of the question, due to the impossibly short distance scale at which quantum gravitational effects are known to be important. Furthermore, string theory contains a stupendous number of vacua, with no known principle for selecting the one we should live in, and so appears to have limited predictive power. Its chief phenomenological success to date is that in many of these vacua, the low-energy effective theory approximately resembles our world, containing the fields of the Standard Model and gravity propagating in 4 large dimensions. A major unsolved difficulty is that all known vacua are supersymmetric, although there are a variety of conceivable ways for the supersymmetry to be broken by a small amount.

As we discuss below, although string theory makes no unique prediction, all known ways of rendering our observations compatible with string theory lead to new, dramatic signals in feasible experiments. In particular, the discovery of branes has led to new possibilities for explaining the gauge hierarchy and the cosmological constant. Many of these can be tested in measurements of gravity at submillimeter scales, or in searches for small deviations from General Relativity at longer distances.

2.2 *Extra dimensions and TeV scale unification of gravity*

2.2.1 “Large” extra dimensions

It is usually assumed that the Planck scale is an actual physical scale, as is the weak scale, and that the gauge hierarchy problem is to explain the origin of two vastly disparate scales. However Arkani-Hamed, Dimopoulos and Dvali (ADD) (54) have proposed an alternative explanation for the weakness of gravity that has stimulated much theoretical and experimental work; see reviews in Refs. (83, 84, 85, 86, 14, 87). ADD conjecture that gravity is weak, not because the fundamental scale is high, but because gravity can propagate in new dimensions of size less than a millimeter. Such “large” new dimensions are not seen by the Standard-Model particles because these are confined to a 3-dimensional subspace of the higher- dimensional theory. Such a framework can be accommodated in string theory (55). A type of p-brane known as a Dp-brane does have gauge and other degrees of freedom as light excitations that are confined to the brane. If the Standard-Model particles are all confined to such a D3-brane, we will not sense additional dimensions except via their modification of the gravitational force law.

The hierarchy problem can be reformulated in this framework. One can assume that the fundamental scale M_* is of order a TeV (56). There is then no hierarchy between the weak scale and M_* , and no gauge hierarchy problem. If there are n new dimensions, the higher-dimensional Newton’s constant $G_{(4+n)}$ can be taken to be

$$G_{(4+n)} = \frac{4\pi}{S_{(2+n)}} \left(\frac{\hbar}{M_* c} \right)^{(2+n)} \frac{c^3}{\hbar} \quad (4)$$

where $S_{(2+n)}$ is the area of a unit $(2+n)$ -sphere,

$$S_{(2+n)} = \frac{2\pi^{(n+1)/2}}{\Gamma\left(\frac{n+1}{2}\right)}. \quad (5)$$

At sufficiently short distances, the gravitational force at a separation r would be proportional to $G_{(4+n)}/r^{2+n}$. To reconcile this with the $1/r^2$ force law observed at long distances, ADD take the n new dimensions to be compact. At distances long compared to the compactification scale the gravitational flux spreads out evenly over the new dimensions, and is greatly diluted. Using Gauss' law, one finds that a for n new dimensions with radius R_* , compactified on a torus, the effective Newton's constant at long distances is

$$G = \frac{\hbar c}{M_*^2} \left[\frac{\hbar}{M_* c} \right]^n \frac{1}{V_n}. \quad (6)$$

where V_n is the volume of the n -torus, $(2\pi R_*)^n$. The relationship between R_* and M_* for other geometries may be found simply by using the appropriate formula for the volume.

The hierarchy problem then becomes transmuted into the problem of explaining the size of the new dimensions, which are much larger than the fundamental scale. There are several proposals for stable compactifications of new dimensions that are naturally exponentially large (57, 58, 59, 60, 61).

To test the ADD proposal directly, one should probe the ISL at a distance scale on the order of R_* . Compact new dimensions will appear as new Yukawa-type forces, of range R_* , produced by the exchange of massive spin-2 particles called Kaluza-Klein (KK) gravitons (62, 63, 64). To see this, note that the components of the graviton momenta in the compact dimensions must be quantized. For instance, compactification of a flat 5th dimension on a circle of radius R would impose the condition on P_5 , the 5th component of the graviton momentum, $P_5 =$

$j\hbar/R$, where j is an integer. The dispersion relation for a massless particle in 5 Lorentz invariant dimensions is

$$E^2 = \sum_{i=0}^3 c^2 P_i^2 + c^2 P_5^2 . \quad (7)$$

Comparing with the 4-dimensional massive dispersion relation

$$E^2 = \sum_{i=0}^3 c^2 P_i^2 + c^4 M^2 . \quad (8)$$

we see that the 5th component of the momentum appears as a 4-dimensional mass term. A 5-dimensional graviton thus appears as an infinite number of new massive spin-2 particles. For a flat new dimension compactified on a circle of radius R , the mass m_j of the j th KK mode is $m_j = j\hbar/(Rc)$ with $j = 1, 2, \dots$

In factorizable geometries (whose spacetimes are simply products of a 4-dimensional spacetime with an independent n -dimensional compact space) the squared wave functions of the KK modes are uniform in the new dimensions. Low-energy effective-field theory analyses of the KK modes and their couplings (65, 66, 67, 68) show that higher-dimensional general coordinate invariance constrains this effective theory. Even at distances less than R , KK mode exchange will not violate the Equivalence Principle. The leading terms in an expansion in $1/M_*$ contain a universal coupling of each graviton KK mode $G_{\mu\nu}^j$ to the stress tensor of form

$$-\sqrt{\frac{8\pi}{M_P}} \sum_j G_{\mu\nu}^j T^{\mu\nu} \quad (9)$$

that is, each KK mode simply couples to the stress tensor in the same manner as the graviton. To compute the correction to the ISL for non-relativistic sources at long distances it suffices to consider the correction to the potential from the exchange of the lightest KK gravitons. The propagators for the KK states may be found in Refs. (65, 66, 67, 68).

For n new dimensions compactified on a flat torus, with the same radius R_* for each dimension, the lowest lying KK mode has multiplicity $2n$ and Compton wavelength R_* . Direct searches for such new dimensions would observe such KK gravitons via the contribution of their lowest-lying modes to the Yukawa potential of Eq. 2, giving $\alpha = 8n/3$ and $\lambda = R_*$. A factor of $4/3$ occurs in α because a massive spin-2 particle has 5 polarization states, and the longitudinal mode does not decouple from a non-relativistic source ¹ Other compact geometries will give similar effects, although the value of α is quite model-dependent.

Assuming all new dimensions are compactified on a torus of radius R_* , and $M_* = 1$ TeV, Eq. 6 gives

$$R_* \approx \frac{1}{\pi} 10^{-17 + \frac{32}{n}} \text{ cm} .$$

The case $n = 1$, $R_* = 3 \times 10^{12}$ m, is clearly ruled out. The case $n = 2$, $R_* = 0.3$ mm, is inconsistent with the results of Ref. (69). It has been shown that this case is even more strongly constrained by the observation of the neutrinos from supernova 1987A (70, 71, 72, 73, 74). Gravitational radiation into the extra dimensions would rapidly cool the supernova before the neutrinos could get emitted, placing a constraint $R_* < 0.7 \mu\text{m}$. The extra gravitational degrees of freedom also necessarily spoil the successful calculations of big-bang nucleosynthesis unless $R_* < 2 \mu\text{m}$, and the decay of the KK modes would add a diffuse background of cosmological gamma rays whose non-observation implies $R_* < 0.05 \mu\text{m}$ (75). For $n \geq 3$, R_* is less than about a nanometer, which is still allowed by astrophysics, cosmology, and direct searches.

¹Note that Refs. (78, 79) included a contribution from a massless “radion” (**gravitational** scalar) in their Newtonian potential, and the radion KK modes in the Yukawa potential, leading to a different value for α . We discuss the radion and why it should be massive later in this section.

It might, therefore, seem that direct observation of the new dimensions in ISL tests is out of the question. However, this conclusion is false. Astrophysical and cosmological bounds are still consistent with a single extra dimension of size 1 mm—in such a scenario the hierarchy problem might be solved via the existence of several more much smaller new dimensions (76). Furthermore, as discussed in the next section, it is easy to alter Eq. 6 and the predictions for higher-dimensional graviton emission. Finally there is a strong argument that the ADD proposal should modify the ISL at a scale of order $\hbar M_P / (cM_*^2)$.

In theories of gravity, the geometry of spacetime is dynamical, and can fluctuate. In particular, the radius of new dimensions can fluctuate independently at each point in our 4-dimensional spacetime. Thus low-energy effective theories of compact extra dimensions inevitably contain spin-0 fields parameterizing the radii of the new dimensions. If the size of the new dimensions is not determined by dynamics, then the linear combination of these fields that determines the extra dimensional volume is a massless Brans-Dicke scalar with gravitational strength coupling, known as the “radion”. A massless radion is decisively ruled out by tests of General Relativity(77). Stabilization of the volume of the extra dimensions is equivalent to a massive radion. Since with a low fundamental scale, the effective potential for the radion should not be much larger than $\mathcal{O}(M_*^4)$, and its couplings are proportional to G_N , the radion mass-squared should be lighter than $\mathcal{O}(G_N M_*^4)$. The radion will mediate a new, gravitational strength force, with $\alpha = n/(n + 2)$ (Ref. (82), and G. Giudice, R. Rattazzi, N. Kaloper, private communications). In many cases the radion is the lightest state associated with new dimensions. For M_* less than a few TeV, its range should be longer than of order 100 microns. Even for relatively “small” new dimensions with size of or-

der an inverse TeV, the radion will, under certain assumptions, have a Compton wavelength in the vicinity of a hundred microns(80, 81).

2.2.2 Warped extra dimensions

The previous discussion assumed the metric for the new dimensions is factorizable. However, the most general metric exhibiting 4-dimensional Poincare invariance is a “warped product”,

$$ds^2 = f(\xi_i)\eta_{\mu\nu}dx^\mu dx^\nu + g_{ij}(\xi_i)\xi_i\xi_j \quad (10)$$

where the ξ_i are the coordinates of the new dimensions, and f and g are general functions of those coordinates. Solving the higher-dimensional Einstein equations for a spacetime with an embedded brane with nonvanishing tension typically requires warping. The “warp factor” $f(\xi_i)$ may be thought of as a ξ -dependent gravitational redshift factor that leads to a potential term in the graviton wave equation. This potential can have a dramatic effect on the ξ dependence of the wavefunctions of the graviton, the graviton KK modes, and the radion.

Randall and Sundrum(88) (RSI) noted that a large hierarchy can be obtained with a single small new dimension if the metric takes the form

$$ds^2 = e^{-2kr_c\xi}\eta_{\mu\nu}dx^\mu dx^\nu + r_c^2 d\xi^2, \quad (11)$$

where ξ is a coordinate living on the interval $[0, \pi]$, k is a constant, and r_c is the compactification scale. This is just the metric for a slice of 5-dimensional anti-deSitter space (maximally symmetric spacetime with constant negative curvature), and is a solution to the 5-dimensional Einstein equations with 5-dimensional Newton’s constant $1/M_*^3$ if there is a negative cosmological constant of size $\Lambda = -24M_*^3 k^2$, and if 3-branes are located at $\xi = 0$ and $\xi = \pi$ with tensions

$\pm 24M_*^3k$. A negative-tension brane seems unphysical, but such bizarre objects can be constructed in string theory, provided the spaces on each side of the brane are identified with each other, that is, the brane represents a boundary condition on the edge of space. For large kr_c , most of the extra-dimensional volume of this space is near the positive-tension brane at $\xi = 0$.

To study the long-distance behavior of gravity in such a spacetime, one examines the behavior of small fluctuations of this metric of the form

$$ds^2 = e^{-2kr_c\xi}[\eta_{\mu\nu} + h_{\mu\nu}(x)]dx^\mu dx^\nu + r_c^2 d\xi^2 . \quad (12)$$

Here $h_{\mu\nu}$ is the 4-dimensional graviton. Plugging this metric into Einstein's equations and linearizing in h , one finds h is a zero mode, or massless solution to the equations of motion, whose wavefunction in the compact dimension simply follows the warp factor $e^{-2kr_c\xi}$. Thus there is a massless 4-dimensional graviton that is localized about the brane at $\xi = 0$ and exponentially weakly coupled to matter on the brane at $\xi = \pi$. If we further hypothesize that the latter brane is where the Standard Model lives, the weakness of gravity is explained for a moderate value of $kr_c \sim 12$. Both k and r_c^{-1} can be of the same order of magnitude as the fundamental scale, and so there is no large hierarchy in the input parameters.

As in the ADD case, the RSI model has a radion parameterizing the compactification scale. Goldberger and Wise (89) have shown that kr_c in the desired range can naturally be stabilized without large dimensionless inputs if the theory contains a massive scalar that lives in the bulk and has source terms localized on the branes. The radion then acquires a large mass of order 100 GeV. The curvature in the extra dimension has a huge effect on the KK graviton spectrum and couplings. The lightest KK modes have masses in the TeV region and large wave

functions near our brane, and therefore $\mathcal{O}(1)$ couplings to ordinary matter. This model has unusual experimental signatures at colliders(14), but is not testable with feasible probes of the ISL.

The RSI model teaches us that warping can have significant effects on phenomenology of the new dimensions. The coupling strength and masses of both the KK modes and the radion can be altered, and the graviton can be localized, or bound to a brane. Furthermore, warping is a generic phenomenon that should also occur in the ADD scenario. Even a very small amount of warping can greatly alter the coupling of the zero-mode graviton to our brane, making this coupling either much stronger or much weaker than for the case of flat extra dimensions (90), altering the relation of Eq. 6. Even in the case of $M_* = 1$ TeV and $n = 2$, with a very small amount of warping, the masses of the lightest KK modes can be either higher or lower than the inverse-millimeter scale predicted by the unwarped case.

2.3 *Infinite-volume extra dimensions*

In a second paper(91), Randall and Sundrum (RSII) explored phenomenology of a graviton zero-mode that is localized about a 3-brane embedded in a noncompact, infinite extra dimension. They found that although 5-dimensional gravity persists at all distance scales, with no gap in the KK spectrum, at long distances the $1/r^2$ force mediated by the zero-mode which is bound to the brane dominates, and the extra dimension can be unobservable at low energy. A simple model of this effect is given by the metric

$$ds^2 = e^{-2k|z|} \eta_{\mu\nu} dx^\mu dx^\nu + dz^2, \quad (13)$$

where z , the coordinate of the 5th dimension, is noncompact. This metric, which represents two slices of anti-deSitter space glued together at $z = 0$, also solves Einstein's equations, provided there is a negative bulk cosmological constant $-24M_*^3k^2$, and a single 3-brane at $z = 0$ of positive tension $24M_*^3k$. The total gravitational potential between two masses m_1 and m_2 separated by a distance r on the brane may be found by summing up the contributions of the bound-state mode and the continuum KK spectrum, which, for distance scales longer than $1/k$, gives

$$V(r) = G_N \frac{m_1 m_2}{r} \left(1 + \frac{1}{r^2 k^2} \right) \quad (14)$$

with $G_N = \hbar^2 k / M_*^3$. The experimental upper bound on $1/k$ from $N = 3$ terms in Eq. 3 has not been explicitly computed, but should be similar to the bound on the radius of an extra dimension. Therefore M_* must be larger than about 10^9 GeV, and there is still a gauge hierarchy. With 2 or more infinite new dimensions, and a graviton confined to our 3-brane, it is possible to lower M_* to a TeV (92). In such a scenario, the weakness of gravity is due to the zero-mode graviton wavefunction spreading over the extra dimensions, as in the ADD proposal, but the width of the wave function is set by the curvature scale rather than by the size of the dimension. Empirically, the main distinction between such weak localization and a large new dimension is that there is no gap in the KK spectrum and the ISL is modified by additional power-law corrections rather than by new Yukawa forces.

The RSI explanation of the weakness of gravity—we live on a brane, the graviton is confined to a different, parallel brane and its wave function here is small—can also be realized in infinite extra dimensions (92, 93). Lykken and Randall studied such a configuration with a single extra dimension and concluded that the weakness of gravity could be explained without input of any large dimensionless

numbers. The chief test of their scenario would be strong emission of graviton KK modes at a TeV collider. The continuum of KK modes would modify the ISL, but their effect would only be significant for distances smaller than ~ 10 fm.

2.4 Exchange forces from conjectured new bosons

Even if new dimensions are absent or small, the ISL can be modified at accessible distance scales by the exchange of new spin-0 or spin-1 bosons; spin-0 bosons would mediate an attractive Yukawa force while spin-1 bosons give a repulsive modification. Here we review some general considerations that apply to such particles, and motivations for considering their existence.

2.4.1 Scalars: general theoretical considerations

In order for a scalar particle, ϕ , to exert a coherent force on matter it must have a Yukawa coupling to electrons, u , d or s quarks, the square of the gluon field strength, or to higher dimension operators such as certain four-quark operators.

The candidates of lowest dimension are

$$\frac{m_e}{f}\phi\bar{e}e, \quad \frac{m_d}{f}\phi\bar{d}d, \quad \frac{m_u}{f}\phi\bar{u}u, \quad \frac{1}{f}\phi G_{\mu\nu}^a G^{a,\mu\nu}. \quad (15)$$

When embedded in the standard model, these all arise from dimension-5 operators, hence the common factor of $1/f$, where f has dimensions of mass. We have assumed that all chiral-symmetry-breaking operators should be proportional to fermion masses. With this assumption, and with all of the above operators present, the gluon coupling will dominate the scalar coupling to matter. Since the matrix element of G^2 in a nucleon is roughly the nucleon mass, M_N , such an interaction would lead to a Yukawa potential of the form given in Eq. 2 with $\lambda = \hbar/(m_\phi c)$ where m_ϕ is the scalar mass and $\alpha \simeq M_P^2/(4\pi f^2)$.

An interaction $(\phi/f)G^2$ produces radiative corrections to m_ϕ . In the standard model with cutoff Λ , one finds

$$\delta m_\phi \simeq \frac{\Lambda^2}{4\pi f} \lesssim m_\phi . \quad (16)$$

Naturalness requires that this be no larger than m_ϕ . For $f = M_N$ and $m_\phi = 2 \times 10^{-4}$ eV, corresponding to a Compton wavelength of 1 millimeter, naturalness implies $\Lambda \lesssim 5$ TeV. This scale Λ approximately coincides with the scale at which naturalness of the electroweak breaking sector demands new physics. A more weakly coupled scalar would correspond to a higher value for Λ .

2.4.2 Forces from axion exchange

A major loophole in the above arguments is that the interactions between matter and a new scalar may not arise from any of the operators in Eq. 15, but rather from nonperturbative QCD effects. This is the case for the pseudoscalar axion invented to explain why strong interactions conserve CP to high precision. A pseudoscalar particle would normally not produce a Yukawa force between unpolarized bodies, but instantons in the presence of CP violation induce a scalar Yukawa coupling of the axion to matter that melts away above Λ_{QCD} . The softness of that coupling makes the radiative correction to the axion mass insignificant. However, a CP-violating scalar axion Yukawa coupling to matter scales roughly as $m_u \bar{\Theta}_{QCD}/f_a \simeq \bar{\Theta}_{QCD}(m_u m_a)/(m_\pi f_\pi)$, where $m_u \lesssim 5$ MeV is the up quark mass, and $\bar{\Theta}_{QCD} \lesssim 10^{-9}$ (94) is the strong CP-violating angle.

Thus for an axion mass $m_a = 10^{-4}$ eV, the scalar axion coupling is at most about 10^{-4} times gravitational strength. ISL tests with unpolarized bodies probe the square of this coupling so they are quite insensitive to the axion. On the other hand, monopole-dipole tests(95), which search for a CP-violating force between

unpolarized and polarized bodies, are linear in the coupling and should be a more sensitive axion probe.

2.4.3 Scalars: cosmological considerations

A light, weakly interacting particle cannot decay or annihilate within a Hubble time, so its relic energy abundance must be equal to or less than that of the observed dark matter. However the cosmology of scalars presents an important difficulty. A natural potential for a scalar in an effective theory below a cutoff Λ has the form $V \sim \Lambda^4 \hat{V}(\phi/f)$, where $\Lambda \approx \sqrt{m_\phi f}$, and \hat{V} is an arbitrary function that is assumed to contain no large dimensionless numbers. If all scalar couplings are proportional to $1/f$, then the scalar lifetime is of order $4\pi f^2/m_\phi^3$, essentially stable. If at a temperature $T \sim \Lambda$ the thermal average of the scalar potential energy is $\langle V \rangle \sim T^4$, then the scalar field would have a large expectation value, $\phi \sim f$. The infinite-wavelength component of this expectation value will be frozen until the Hubble scale is of order $1/m_\phi$, and will subsequently act like cold dark matter. Assuming the standard-model spectrum and standard cosmology for $T < \Lambda$ (e.g., that the reheat temperature following inflation is above Λ), then an initial scalar energy density of T^4 at $T = \Lambda$ implies a ratio today of the energy in cold scalars to the energy in baryons of order

$$\frac{\rho_w}{\rho_B} \simeq 2 \times 10^8 \left(\frac{\Lambda}{M_N} \right), \quad (17)$$

which is clearly unacceptable.

Cosmology with light scalars can be made acceptable by invoking a very late stage of inflation with Hubble constant H less than or of order m_ϕ . Then ϕ rapidly evolves to the minimum of its potential. Once inflation ends, the universe must reheat to a temperature T_R . However the minimum of the scalar potential at

T_R does not coincide with the minimum today, due to the tadpole generated by the interactions Eq. 15 at finite temperature. One must therefore check that coherent scalar oscillations do not get regenerated during the reheating process after inflation. If the reheating causes the minimum of the potential to change suddenly on a timescale compared with the oscillation time (of order 10^{-13} s), then regeneration of the scalar condensate can be significant. We are almost completely ignorant of both the late inflationary mechanism and the reheating timescale t_R , but a rough bound on t_R may be estimated from the reheating temperature using the sudden inflaton decay approximation

$$t_r \sim (2/3)H^{-1} \sim (2/3) \left(\frac{M_P}{T_R} \right) \left(\sqrt{\frac{90}{8\pi^3 g_*}} \right). \quad (18)$$

For $T_R \gtrsim 10$ MeV, which is necessary for standard big-bang nucleosynthesis, $t_r \sim 3 \times 10^{-3}$ s. Much higher reheat temperatures might be necessary to generate the baryon number asymmetry. For example, a reheat temperature of order 100 GeV corresponds to a reheat time of order $t_r \sim 3 \times 10^{-11}$ s.

Provided this timescale is much longer than the scalar oscillation time $\hbar/(m_\phi c^2)$ the evolution of the minimum of the potential can take place adiabatically, injecting little energy into the coherent mode. The requirement of such a late stage of inflation with acceptable reheating places constraints on theories of particle physics near the weak scale, but does not rule out the existence of light scalars.

2.4.4 Bosons from hidden supersymmetric sectors

As we discussed in Section 2, new physics is expected at the TeV scale. One candidate for this new physics is supersymmetry, which is predicted in unified theories, and which can explain the gauge hierarchy. Unbroken supersymmetry predicts an unobserved degeneracy between fermions and bosons, hence super-

symmetry must be broken at a scale of 100 GeV or higher. The most popular scenario involves supersymmetry breaking at a scale of $M_S \sim 10^{11}$ GeV in a “hidden” sector that couples to our visible world only via gravity and interactions of similar strength. The apparent scale of supersymmetry breaking in the visible world would then be of order $M_S^2/M_P \sim 10^3$ GeV. In other scenarios supersymmetry-breaking is communicated to the visible world by the gauge forces of the Standard Model, and the supersymmetry-breaking scale is as low as $M_S \sim 10^4$ GeV. The supersymmetry-breaking scale is linked to $m_{3/2}$, the mass of the gravitino (the spin-3/2 superpartner of the graviton), through the relation $m_{3/2} = M_S^2/M_P$. Well motivated theoretical expectations for the gravitino mass range from an meV to 10^4 GeV. In some scenarios(96, 97, 122, 123) the gravitino mass may be linked with the size of the cosmological constant inferred from the supernova observations and should be about an meV.

If there are hidden sectors—particles coupled to the visible sector only via gravitational strength interactions—the apparent scale of supersymmetry breaking in those sectors would typically be of order $m_{3/2}$. Scalar particles from those sectors could naturally have a mass in the meV range and mediate gravitational strength forces with a range of of order 100 microns.

Note that the severe cosmological problems typical of light weakly coupled scalars discussed in the previous section do not necessarily occur for a scalar that is part of a hidden supersymmetric sector exhibiting supersymmetry down to the meV scale. Such scalars might have a potential coming from $\mathcal{O}(1)$ couplings to particles in this sector, while maintaining a naturally small mass and gravitational-strength couplings to particles in the visible sector. These couplings will allow for the scalar field to relax to its minimum and for particle decay and

annihilation.

2.4.5 Forces from exchange of stringy bosons

Supersymmetric hidden sectors are ubiquitous in string theory. All known acceptable vacua of string theory are supersymmetric, and contain a tremendous number of “moduli”—massless scalar fields whose expectation values set the parameters of the effective theory. These moduli are extremely weakly coupled, with couplings inversely proportional to the fundamental scale. In order to give these fields a mass, it is necessary to break supersymmetry, however moduli necessarily couple weakly to the supersymmetry-breaking sector and, for a low supersymmetry-breaking scale, are expected to be extremely light. Current understanding is inadequate to predict the moduli masses, but a rough estimate suggests these should be of order $m_{3/2}$ (98). The best way to look for moduli is therefore to test the ISL at submillimeter distance scales. The couplings of the moduli in any given vacuum are computable, and so there are definite predictions. The best-understood scalar is the dilaton, a modulus that determines the strength of the gauge couplings. Its couplings to ordinary matter can be determined and are nearly free of QCD uncertainties, so its discovery could provide a genuine smoking gun for string theory (99).

2.4.6 Forces from the exchange of weakly coupled vector bosons

A new **repulsive** Yukawa interaction would be a signal for the exchange of a massive spin-1 boson, presumably a gauge particle. In the ADD scenario, any gauge fields that propagate in the bulk of the new dimensions would have their couplings diluted by the same volume factor as the graviton and so would mediate a force

with similar strength. Actually, since the gravitational force is also weakened by the smallness of the M_N relative to M_* , one would expect any such gauge forces to be stronger than gravity by a very large factor of $(M_*/M_N)^2 \sim 10^6\text{--}10^8$. This is acceptable if the range is substantially shorter than a millimeter (see Sec. 4.4.3) Gauge bosons could have a mass in an interesting range if the symmetry is broken via a scalar condensate on a brane. The resulting mass will be diluted by the bulk volume as well, and would naturally be in the range $M_*/(VM_*^3) \sim M_*^2/M_P$. For M_* of order a few TeV, the range would be about a hundred microns(70). If the symmetry breaking occurs on the brane we live on, the gauge boson couplings to standard model matter could be substantially suppressed (102).

Compactifications of string theory and other extra-dimensional theories often contain new massless spin-1 particles, known as graviphotons, that arise from components of the higher- dimensional graviton. These generally do not couple to ordinary light matter, but it has been suggested that such bosons might acquire small masses and small, gravitational-strength couplings to ordinary matter, e.g. by mixing with other vector bosons (100, 101, 104, 105). Light spin-1 bosons do not suffer from the naturalness or cosmological difficulties of scalar particles, provided that they couple to conserved currents. However, spin-1 (and spin-0) boson exchange necessarily “violates” the Equivalence Principle and the couplings of bosons with masses less than $1 \mu\text{eV}$ are strongly constrained by the experiment of Ref.(106).

2.5 Attempts to solve the cosmological constant problem

Comprehensive reviews of the cosmological constant problem and the many attempts to solve it can be found in Refs. (107, 108, 109, 29, 110). Recent theo-

retical activity on this topic has been intense but is still inconclusive. We will not attempt an exhaustive discussion of this issue, but will simply mention a few of the interesting recent proposals that imply modifications of the ISL at long distances.

Beane (30) pointed out that in any local effective quantum field theory, naturalness would imply new gravitational physics at a distance scale of order a millimeter that would cut off shorter distance contributions to the vacuum energy. Sundrum (31) has speculated about the sort of effective theory that might do this. Sundrum proposed that the graviton is an extended object, with size of order a millimeter, and has been exploring how to construct a natural and viable effective field theory arising from this picture (31, 111). It is still not clear how self-consistent this effective theory is, but it does have the great virtue of making a definite, testable experimental prediction—gravity should shut off below a distance scale of order a 100 microns.

Many people have attempted to use extra dimensions to explain the smallness of cosmological constant, motivated by the alluring observation (112) that in higher-gravitational theories with branes, the 4-dimensional vacuum energy or brane tension does not necessarily act as a source of 4-dimensional gravity, but can instead lead to curvature only in the new dimensions. So far no solved, consistent example actually yields a small cosmological constant in the 4-dimensional effective description without extreme finetuning or other problematic features.

Theories with branes and noncompact new dimensions allow for another surprising phenomenon known as quasi-localization of gravity (113, 114, 115, 116). In these theories, as in RSII, long-distance gravity is higher dimensional. However there is no zero-mode bound to our 3-brane. There is, instead, a metastable

quasi-bound state that propagates 4-dimensionally along the brane over times and distances short compared to some maximum scale. The ISL, and 4-dimensional General Relativity, will approximately apply from r_{\min} to r_{\max} , but not to arbitrarily long distances. The consistency of various theories of quasi-localization is still under debate and the theories themselves have been rapidly mutating.

The holographic principle insinuates that a local description of a gravitational theory must break down somehow, since there are not enough degrees of freedom to allow for independent observables at different space-time points. Several theorists have speculated that the breakdown of locality might even occur in a subtle way at astronomical or even longer distances, and that this might explain the size of the cosmological constant (117, 118, 119, 120, 121). In the scenario of Banks (117, 120, 122, 123), supersymmetry ends up being broken at a scale of a few TeV by nonlocal effects due to the cosmological constant, leading to masses for the gravitino, dilaton and other moduli of order meV and deviations from the ISL at 100 microns.

Many of the above ideas share the possibility that there is some scale r_{\max} , beyond which Einstein gravity gets modified. Modifying gravity at long distance allows for a new approach to the cosmological constant. The observed acceleration of the universe might be caused by a change in the behavior of gravity at the Hubble scale, instead of by dark energy(124). The prospect that the effective Newton's constant might be strongly-scale dependent at large distance scales (gravity as a "high-pass spatial filter") is fascinating, and leads to a new view of the cosmological constant problem. Conventionally it is assumed that the vacuum energy gravitates so weakly because, for some mysterious reason, this energy is actually very small. But if the strength of gravity depends on the wavelength of

the source, it becomes credible that the vacuum energy is indeed very large, but that it gravitates weakly because it is very smooth. Ideas along these directions have been pursued in Refs.(125, 126, 127).

Refs. (128, 129, 130, 131, 132) present an intriguing assertion about theories of quasi-localization that may account for the acceleration of the universe. For any localized gravitational source, there exists a distance scale r_* , which is a function of the gravitational radius of the source and r_{\max} , beyond which the graviton will acquire an extra polarization state that couples to the source so that the strength of gravity will change. This scale r_* decreases for less massive gravitating objects. Dvali, Gruzinov and Zaldarriaga(132) argue that ultra-precise measurements of the anomalous precession of the perihelion of planetary orbits can test models of quasi-localization that explain the cosmological acceleration. For instance a 17-fold improvement this measurement in the Earth-Moon system via LLR, would test a particular model in Ref.(132).

3 EXPERIMENTAL CHALLENGES

3.1 *Signals*

The dominant problem in testing gravitation at short length scales, is the extreme weakness of gravity. This forces the experimenter to adopt designs that maximize the signal and minimize backgrounds and noise. For example, one could measure the force between spheres as was done by (133), between cylinders as was done in (134) and (135), between a sphere and a plane as was done in (136) and (137), or in planar geometry as was done by (69) and (138). Clearly, at a given minimum separation, the signal from a short-range interaction, per unit test-body mass, is least for 2 spheres and greatest for 2 planes.

The Yukawa force between two spheres of radii r_1 and r_2 and masses m_1 and m_2 , whose centers are separated by s , is

$$F_Y = \alpha G m_1 m_2 \Phi\left(\frac{r_1}{\lambda}\right) \Phi\left(\frac{r_2}{\lambda}\right) \left(1 + \frac{s}{\lambda}\right) \frac{e^{-s/\lambda}}{s^2}, \quad (19)$$

where $\Phi(x) = 3(x \cosh x - \sinh x)/x^3$. For $x \gg 1$, $\Phi(x) \approx 3e^x/(2x^2)$, while for $x \ll 1$, $\Phi(x) \approx 1$. Therefore, for $\lambda \ll r$, the ratio of Yukawa to Newtonian forces for two spheres of radius r separated by a gap d is

$$\frac{F_Y}{F_N} \approx \alpha \frac{9 \lambda^3}{2 r^3} \left(1 + \frac{d}{2r}\right) e^{-d/\lambda}. \quad (20)$$

The potential energy from a Yukawa interaction between a flat plate of area A_p , thickness t_p and density ρ_p a distance d from an infinite plane of thicknesses t , and density ρ , is

$$V_Y = 2\pi\alpha G \rho_p \rho \lambda^3 A_p [1 - e^{-t_p/\lambda}] [1 - e^{-t/\lambda}] e^{-d/\lambda}, \quad (21)$$

if end effects are neglected. The corresponding force is

$$F_Y = 2\pi\alpha G \rho_p \rho \lambda^2 A_p [1 - e^{-t_p/\lambda}] [1 - e^{-t/\lambda}] e^{-d/\lambda}. \quad (22)$$

In this case, for λ much less than the thicknesses, the force ratio becomes

$$\frac{F_Y}{F_N} \approx \alpha \frac{\lambda^2}{t_p t} e^{-d/\lambda}. \quad (23)$$

The potential energy of a Yukawa interaction between a sphere of radius r and mass m above an infinite plane of thickness t and density ρ_p is

$$V_Y = \pi\alpha G m \rho \lambda^2 \Phi(r/\lambda) e^{-s/\lambda} \quad (24)$$

where s is the distance from the center of the sphere to the plane. The corresponding force is $F_Y = \pi\alpha G m \rho \lambda \Phi(r/\lambda) e^{-s/\lambda}$. In this case, for $\lambda \ll r$, the force ratio becomes

$$\frac{F_Y}{F_N} \approx \alpha \frac{3 \lambda^3}{4 r^2 t} e^{-d/\lambda} \quad (25)$$

where d is the gap between the spherical surface and the plane.

3.2 Noise considerations

Thermal noise in any oscillator sets a fundamental limit on the achievable statistical error of its amplitude. A single-mode torsion oscillator subject to both velocity and internal damping obeys the equation

$$\mathcal{T} = I\ddot{\theta} + b\dot{\theta} + \kappa(1 + i\phi)\theta, \quad (26)$$

where \mathcal{T} is the applied torque, I the rotational inertia, θ the angular deflection of the oscillator, and κ the torsional spring constant of the suspension fiber. The velocity-damping coefficient b accounts for any losses due to viscous drag, eddy currents etc., while the loss angle ϕ accounts for internal friction of the suspension fiber. We compute the spectral density of thermal noise following Saulson's (147) treatment based on the fluctuation-dissipation theorem. The spectral density of torque noise power (per Hz) at frequency ω is

$$\langle \mathcal{T}_{\text{th}}^2(\omega) \rangle = 4k_B T \Re(Z(\omega)) \quad (27)$$

where k_B is Boltzmann's constant, T the absolute temperature, and $Z = \mathcal{T}/\dot{\theta}$ is the mechanical impedance.

First consider the familiar case of pure velocity damping ($b > 0$, $\phi = 0$) where $Z(\omega) = iI\omega + b + \kappa/(i\omega)$. In this case, the spectral density of torque noise,

$$\langle \mathcal{T}_{\text{th}}^2(\omega) \rangle = 4k_B T \frac{I\omega_0}{Q} \quad (28)$$

($\omega_0 = \sqrt{\kappa/I}$ is the free resonance frequency and $Q = I\omega_0/b$ the quality factor of the oscillator) is independent of frequency. The corresponding spectral density of angular deflection noise in θ is

$$\langle \theta_{\text{th}}^2(\omega) \rangle = \frac{4k_B T}{QI} \frac{\omega_0}{(\omega_0^2 - \omega^2)^2 + (\omega_0\omega/Q)^2}. \quad (29)$$

Note that the integral of Eq. 29 over all $f = \omega/(2\pi)$ is $k_B T/\kappa$, consistent with the equipartition theorem. The signal due to an external torque \mathcal{T} is

$$|\theta(\omega)| = \frac{\mathcal{T}}{I} \frac{1}{\sqrt{(\omega_0^2 - \omega^2)^2 + (\omega\omega_0/Q)^2}} \quad (30)$$

so that the signal-to-noise ratio in unit bandwidth has the form

$$S(\omega) = \frac{|\theta(\omega)|}{\sqrt{\langle\theta_{\text{th}}^2\rangle + \theta_{\text{ro}}^2}} = \frac{\mathcal{T}}{\sqrt{4k_B T \omega_0 I/Q + \langle\theta_{\text{ro}}^2\rangle I^2 ((\omega_0^2 - \omega^2)^2 + (\omega\omega_0/Q)^2)}} \quad (31)$$

where we have included a noise contribution $\langle\theta_{\text{ro}}^2\rangle$ from the angular deflection readout system. The signal is usually placed at a frequency $\omega \leq \omega_0$ to avoid attenuating the deflection amplitude θ because of oscillator inertia.

Now consider the case of pure internal damping ($b = 0$, $\phi > 0$) where $Z = iI\omega + \kappa/(i\omega) + \kappa\phi/\omega$. In this case the spectral density of thermal noise has a $1/f$ character,

$$\langle\mathcal{T}_{\text{th}}^2(\omega)\rangle = 4k_B T \frac{I\omega_0^2}{\omega Q} \quad (32)$$

where now $Q = 1/\phi$. The corresponding spectral density of thermal noise in the angular deflection is

$$\langle\theta_{\text{th}}^2\rangle = \frac{4k_b T}{Q\omega I} \frac{\omega_0^2}{(\omega_0^2 - \omega^2)^2 + (\omega_0^2/Q)^2} . \quad (33)$$

The signal-to-noise ratio in unit bandwidth is

$$S = \frac{\mathcal{T}}{\sqrt{4k_B T I \omega_0^2 / (Q\omega) + \langle\theta_{\text{ro}}^2\rangle I^2 ((\omega_0^2 - \omega^2)^2 + (\omega_0^2/Q)^2)}} \quad (34)$$

so that it is advantageous to boost the signal frequency above ω_0 until θ_{ro}^2 makes a significant contribution to the noise.

3.3 Backgrounds

Electromagnetic interactions between the test bodies are the primary source of background signals and may easily dominate the feeble gravitational signal. In the

following sections, we discuss the dominant electromagnetic background effects in ISL experiments.

3.3.1 Electric potential differences and patch fields

Electric charges residing on insulating or ungrounded test bodies are difficult to quantify and Coulomb forces acting on such bodies can exceed their weights. For this reason, ISL tests typically employ conducting grounded test bodies. Even so, a variety of effects can give the test bodies different electric potentials. If dissimilar materials are used for the test bodies, a potential difference equal to the difference between the work functions of the two materials is present, typically of order of 1 V. Even if the same material is used for both test bodies or the test bodies are both coated with the same material, such as gold, small differences in the contact potentials connecting the test bodies to ground can leave a net potential difference between the test bodies. With care, such contact potential differences can be reduced to the level of a few mV(139).

Neglecting edge effects, the attractive electric force between a conducting plate with area A parallel to an infinite conducting plate is $F_E(d) = \epsilon_0 AV^2/(2d^2)$, where d is the separation between the plates, V is the potential difference between the plates and ϵ_0 is the permittivity of free space. For 1 mm thick plates with a density of 10 g/cm³, separated by 0.1 mm, F_E becomes as large as F_N for a potential difference of 10 mV, and the electric force grows with decreasing separation while the Newtonian force is constant.

Even if test bodies are at the same average potential, they experience a residual electric interaction from patch fields—spatially varying microscopic electric potentials found on the surface of materials(140). Patch fields arise because different

crystal planes of a given material have, in general, different work functions(141) that can, in extreme cases be as big as 1 V. To the extent that the surface is a mosaic of random microscopic crystal planes, there will be local potential differences with a scale size comparable to the size of the microcrystals. For example, different planes of W crystals have work functions that vary by 0.75 V. Gold is a good choice for test body coating as the work functions of its crystal planes vary by only 0.16 V. Surface contaminants also contribute to the local variation of the electric potential, altering the local work function and providing sites for the trapping of electrical charge. In the limit that the patches are smaller than the separation, the patch field force(140) scales as $1/d^2$.

3.3.2 Casimir Force

Vacuum fluctuations of the electromagnetic field produce a fundamental background to ISL tests at short length scales. The Casimir force(142) between objects in close proximity may be viewed as arising either from the modification of the boundary conditions for zero-point electromagnetic modes or from the force between fluctuating atomic dipoles induced by the zero-point fields(143). The Casimir force can be quite large compared to the force of gravity. The Casimir force between two grounded, perfectly conducting, smooth, infinite planes at zero temperature, separated by a distance d , is attractive

$$\frac{F_C}{A} = \frac{\pi^2 \hbar c}{240d^4} . \quad (35)$$

For a 1 mm thick plate of area A near an infinite plate of thickness 1 mm (again, both with density 10 g/cm³), F_C becomes equal to F_N at a separation of $d = 13$ microns.

Because of the difficulty of precisely aligning two parallel planes that involves

4 degrees of freedom, experimenters usually measure the force between a sphere (or spherical lens) and a plane. Assuming perfectly conducting, smooth bodies at zero temperature, the Casimir force is attractive with a magnitude

$$F_C = \frac{\pi^3 R \hbar c}{360 d^3} \quad (36)$$

where R is the radius of the sphere and d is the minimum separation between the surfaces of the sphere and plane. For a 1 mm radius sphere near an infinite 1 mm thick plane (both with a density of 10 g/cm³) F_C becomes equal to F_N at a separation $d = 2.5$ microns.

The Casimir force expressions in Eqs. 35 and 36 must be corrected for finite temperature, finite conductivity, and surface roughness (see below). All these corrections vary with the separation, d , making it difficult to isolate a gravitational anomaly from an electrical effect.

3.3.3 Electrostatic shielding

Fortunately, backgrounds from Casimir, electric potential differences and patch-effect forces can be greatly reduced by using a moving “attractor” to modulate the signal on a stationary “detector” and placing a stationary, rigid, conducting membrane between the “detector” and the “attractor”. But this electrostatic shield places a practical lower limit of some 10’s of μm on the minimum attainable separation between the test bodies.

3.3.4 Magnetic effects

Microscopic particles of iron imbedded in nominally nonmagnetic test bodies during their machining or handling, or in the bulk during smelting, can create local magnetic fields so small they are difficult to detect with standard magnetome-

ters, yet large enough to compete with gravitational forces. The magnetic force between two magnetically saturated iron particles, 1 mm apart, each 10 microns in diameter can be as large as 10^{-7} dynes, varying as the inverse fourth power of the distance between the particles. This is as large as the gravitational attraction between a 1 mm thick Al plate with an area of 3 cm^2 near an infinite Al plate that is 1 mm thick. Yet the magnetic field of such a particle is only 0.3 mGauss at a distance of 2 mm.

Most ISL tests modulate the position of an attractor and detect the force this modulation produces on a detector. Even if the attractor has no ferromagnetic impurities, any magnetic field associated with the attractor modulation, say from motor magnets or flowing currents, can couple to magnetic impurities in the detector. Experimenters typically measure the magnetic field associated with the modulation of the attractor and apply larger fields to find the response of the detector. A variety of smaller magnetic background effects are associated with the magnetic susceptibilities of the test bodies. Standard magnetic shielding of the experimental apparatus is usually sufficient to reduce the ambient magnetic field to a level where the susceptibilities pose no problem.

3.3.5 Other effects

Modulation of the attractor position may introduce background effects that are not electromagnetic. The most obvious is a spurious mechanical coupling whereby the motion of the attractor is transmitted via the apparatus to the detector. These unwanted couplings can be reduced by multiple levels of vibration isolation and by experimental designs that force the signal frequency to differ from that of the attractor modulation. Experiments are performed in vacuum chambers to

reduce coupling between the test bodies from background gas.

3.4 Experimental strategies

ISL tests can be constructed as null experiments, partial-null experiments or as a direct measurements. For example, Ref. (134) studied the force on a cylinder located inside a cylindrical shell. To the extent that the length-to-radius ratios of the cylinders are very large, this constitutes a null-test as the Newtonian interaction between the cylinders gives no net force. Null tests have also been made using planar geometry; the Newtonian force between two parallel, infinite planes is independent of their separation. This basic idea, as discussed below, has been exploited by Ref. (138). Null experiments have the advantage that apparatus does not need to handle signals with a wide dynamic range and the results are insensitive to instrumental non-linearities and calibration uncertainties.

A partial null experiment where the Newtonian signal was largely, but not completely, cancelled has been reported in Ref. (69). As discussed below, the partial cancellation greatly reduced the required dynamic range of the instrument, but Newtonian gravity still gave a very characteristic signal that was used to confirm that the instrument was performing properly, and whose **form** (as well as **magnitude**) provided constraints on new physics.

Finally, Ref. (133) reported a direct experiment that compared the measured force between two spheres as their separation was switched between two values. In this case, the results depended crucially on measuring accurately the separations of the spheres and the forces between them.

4 EXPERIMENTAL RESULTS

4.1 *Low-frequency torsion oscillators*

4.1.1 The Washington experiment

Hoyle et al.(69) at the University of Washington Eöt-Wash group developed a “missing mass” torsion balance, shown in Fig. 1, for testing the ISL at short-ranges. The active component of the torsion pendulum was an aluminum ring with 10 equally spaced holes bored into it. The pendulum was suspended above a copper attractor disk containing 10 similar holes. The attractor was rotated uniformly by a geared down stepper motor. The test bodies in this instrument were the “missing” masses of the two sets of 10 holes. In the absence of the holes, the disk’s gravity simply pulled directly down on the ring and did not exert a twist. But because of the holes, the ring experienced a torque that oscillated 10 times for every revolution of the disk—giving sinusoidal torques at 10ω , 20ω and 30ω , where ω was the attractor rotation frequency. This torque twisted the pendulum/suspension fiber and was measured by an auto-collimator that reflected a laser beam twice from a plane mirror mounted on the pendulum. Placing the signals at high multiples of the disturbance frequency (the attractor rotation frequency) reduced many potential systematic errors. A tightly stretched $20\ \mu\text{m}$ thick beryllium-copper electrostatic shield was interposed between the pendulum and the attractor to minimize electrostatic and molecular torques. The entire torsion pendulum including the mirrors was coated with gold and enclosed in a gold-coated housing to minimize electrostatic effects. The pendulum could not “see” the rotating attractor except for gravitational or magnetic couplings. Magnetic couplings were minimized by machining the pendulum and attractor

with non-magnetic tools and by careful handling.

The experiment was turned into a partial-null measurement by adding a second, thicker copper disk immediately below the upper attractor disk. This disk also had 10 holes bored into it, but the holes were rotated azimuthally with respect to the upper holes by 18 degrees and their sizes were chosen to give a 10ω torque that just cancelled the 10ω Newtonian torque from the upper attractor. On the other hand, a new short-range interaction would not be cancelled because the lower attractor disk was simply too far away from the pendulum. The cancellation was exact for a separation (between the lower surface of the pendulum and the upper surface of the attractor) of about 2 mm. For smaller separations the contribution of the lower disk was too small to completely cancel the 10ω signal, while at larger separations the lower disk's contribution was too large (see Fig. 2).

Two slightly different instruments were employed; both had 10-fold rotational symmetry and differed mainly in the dimensions of the holes. In the first experiment the pendulum ring was 2.002 mm thick with 9.545 mm diameter holes with a total hole "mass" of 3.972 g; in the second experiment the ring thickness was 2.979 mm thick with 6.375 mm diameter holes having a total hole "mass" of 2.662 g. The resonant frequencies of the two pendulums were $\omega_0/2\pi = 2.50$ mHz and 2.14 mHz, respectively and the fundamental 10ω signals were set at precisely $10/17 \omega_0$ and $2/3 \omega_0$, respectively. In both cases the 20ω and 30ω harmonics were above the resonance. The observed spectral density of deflection noise was close to the thermal value given in Eq. 33 for the observed Q-factor of 1500 (see also Fig. 10 below).

4.1.2 Signal scaling relations

The gravitational torque exerted on the pendulum by the rotating attractor is $T_g(\phi) = -\partial V(\phi)/\partial\theta$, where $V(\phi)$ is the gravitational potential energy of the attractor when the attractor is at angle ϕ , and θ is the twist angle of the pendulum. For cylindrical holes, four of the six Newtonian torque integrals can be solved analytically but the remaining two must be evaluated numerically. Clearly the Newtonian signal drops as the number of holes increases and their radii decrease because the long-range gravitational force tends to “average away” the holes. It also drops rapidly for separations much greater than the thickness of the upper attractor disk. Only 3 of the Yukawa torque integrals can be solved analytically. However, when the Yukawa range, λ , becomes much smaller than any of the relevant dimensions of the pendulum/attractor system a simple scaling relation based on Eq. 21 governs the signal and

$$T_Y \propto \alpha G \rho_p \rho_a \lambda^3 e^{-s/\lambda} \frac{\partial A}{\partial \phi} \quad (37)$$

where ρ_p and ρ_a are the densities of the pendulum and attractor, λ is the Yukawa range, and A the overlap area of the holes in the pendulum with those of the attractor when the attractor angle is ϕ .

4.1.3 Backgrounds

The effects from spurious gravitational couplings, temperature fluctuations, variations in the tilt of the apparatus and magnetic couplings were measured and found to be negligible compared to the statistical errors. Electrostatic couplings were negligible because the pendulum was almost completely enclosed by a gold-coated housing. The 20 μm thick electrostatic shield was rigid to prevent secondary electrostatic couplings. The shield’s lowest resonance was about 1 kHz,

and the attractor could only produce a false electrostatic effect by flexing the shield at a very high $m = 10$ mode.

4.1.4 Alignment and calibration

Although all sub-millimeter tests of the ISL face an alignment problem, it was especially important in this experiment because of the relatively large size of the pendulum (chosen to increase the sensitivity). Alignment was done in stages. First the pendulum ring was leveled by nulling its differential capacitance as the pendulum rotated above two plates installed in place of the electrostatic shield. The shield was then replaced and the tilt of the entire apparatus was adjusted to minimize the pendulum-to-shield capacitance. Horizontal alignment was done by measuring the gravitational torque as the horizontal position of the upper fiber suspension point was varied. Determining separations from mechanical or electrical contacts was found to give unreliable results so the crucial separation between the pendulum and the electrostatic shield was determined from the electrical capacitance.

The torque scale was directly calibrated using gravity. Two small aluminum spheres were placed in an opposing pair of the 10 holes of the torsion pendulum and two large bronze spheres, placed on an external turntable, were rotated uniformly around the instrument at a radius of 13.98 cm. Because this was close to the 16.76 cm radius⁽¹⁴⁴⁾ used in determining G and the ISL has been tested at this length scale (see Fig. 9), the calibration torque could be computed to high accuracy. The torsion constant of the fiber was about .03 dyne cm.

4.1.5 Results

Data were taken at pendulum/attractor separations down to $197\mu\text{m}$, where the minimum separation was limited by pendulum “bounce” from seismic disturbances. The torque data, shown in Fig. 2, were analysed by fitting a potential of the form given in Eq. 2 with α and λ as free parameters and treating the important experimental parameters (hole masses and dimensions, zero of the separation scale, torque calibration constant, etc.) as adjustable parameters constrained by their independently measured values. Reference (69) reported results from the first of the two experiments; the combined 95% confidence level result of both experiments was given subsequently(145, 146) and is shown in Fig. 6.

The results exclude the scenario of two equal extra dimensions with a size giving a unification scale of $M^* = 1 \text{ TeV}$; this would imply an effective Yukawa interaction with $\lambda = 0.3 \text{ mm}$ and $\alpha = 16/3$ if the extra dimensions are compactified as a torus. Because $\alpha \geq 16/3$ is consistent with the data only for $\lambda < 130 \mu\text{m}$, Eq. 6 implies that $M_* > 1.7 \text{ TeV}$. A tighter bound on M_* can be extracted from the radion constraint, which in the unwarped case where $1/3 \leq \alpha \leq 3/4$ for $1 \leq n \leq 6$, suggests that $M_* \geq \mathcal{O}(3 \text{ TeV})$.

More interesting and general is the upper limit Ref. (69, 145, 146) places on the size of the **largest single** extra dimension, assuming all other extra dimensions are significantly smaller. For toroidal compactification, this corresponds to the largest λ consistent with $\alpha = 8/3$, leading to an upper limit $R_* \leq 155 \mu\text{m}$. Other compactification schemes necessarily give somewhat different limits.

4.2 *High-frequency torsion oscillators*

4.2.1 The Colorado experiment

The modern era of short-range ISL tests was initiated by Long et al. at the University of Colorado(148). Their apparatus, shown in Fig. 3, used a planar null geometry. The attractor was a small $35 \text{ mm} \times 7 \text{ mm} \times .305 \text{ mm}$ tungsten “diving board” that was driven vertically at 1 kHz in its 2nd cantilever mode by a PZT bimorph. The detector, situated below the “diving board”, was an unusual high-frequency compound torsion oscillator made from 0.195 mm thick tungsten. It consisted of a double-rectangle for which the 5th normal mode resonates at 1 kHz; in this mode the smaller $11.455 \text{ mm} \times 5.080 \text{ mm}$ rectangle (the detector) and the larger rectangle (one end of which was connected to a detector mount) counter-rotated about the torsional axis with the detector rectangle having the larger amplitude. The torsion oscillations were read out capacitively from the larger rectangle. The attractor was positioned so that its front end was aligned with the back edge of the detector rectangle and a long edge of the attractor was aligned above the detector torsion axis. A small electrostatic shield consisting of a .06 mm thick sapphire plate coated with 100 nm of gold was suspended between the attractor and the detector. The attractor, detector and electrostatic shield were mounted on separate vibration-isolation stacks to minimize any mechanical couplings, and were aligned by displacing the elements and measuring the points of mechanical contact.

In any null experiment it is helpful to know the precise form of a signal of new physics. Long et al. did this by sliding away the electrostatic shield and applying a 1.5 V bias to the detector to give a large, attractive electrostatic force; this

determined the phase of the signal that would be produced by a new, short-range interaction.

4.2.2 Signal-to-noise considerations and calibration

The spectral density of thermal force noise in the multi-mode oscillator used in Ref. (148) obeys a relation similar to Eq. 32. The Colorado experimenters operated on a resonance with a $Q = 25,000$ so the readout noise was negligible. Data were taken with the attractor driven at the detector resonance as well as about 2 Hz below the resonance (see Fig. 4). The means of the on-resonance and off-resonance data agreed within errors, but the standard deviation of the on-resonance data was about twice that of the off-resonance data. This is just what one expects if the on-resonance data were dominated by thermal noise. Furthermore, the on-resonance signal did not change as the geometry was varied. This ruled out the unlikely possibility that the observed null result came from a fortuitous cancellation of different effects, all of which should have different dependences on the geometry. The torsion oscillation scale was calibrated by assuming that the on-resonance signal was predominantly thermal.

4.2.3 Backgrounds

Although a net signal was seen, it had the same magnitude on and off-resonance and presumably was due to electronic pickup. No evidence was seen for an additional, statistically significant background. Checks with exaggerated electrostatic and magnetic effects showed that plausible electrostatic and magnetic couplings were well below the level of thermal noise.

4.2.4 Results

The null results from this experiment, taken at a separation of $108 \mu\text{m}$, were turned into $\alpha(\lambda)$ constraints using a maximum-likelihood technique. For various assumed values of λ , the expected Yukawa force was calculated numerically 400 times, each calculation using different values for experimental parameters that were allowed to vary within their measured ranges. A likelihood function was constructed from these calculations and was used to extract 95% level limits on $\alpha(\lambda)$. The results(138), shown in Fig. 6, exclude a significant portion of the moduli forces predicted by Dimopoulos and Giudice(98).

4.3 *Micro-cantilevers*

4.3.1 The Stanford experiment

Chiaverini et al. at Stanford(149, 150) recently reported a test of the ISL using a microcantilever apparatus that was suited for the $10 \mu\text{m}$ length scale, but which did not have the sensitivity to see gravity. The apparatus consisted of a silicon microcantilever with a $50\mu\text{m} \times 50\mu\text{m} \times 50\mu\text{m}$ gold test mass mounted on its free end. The cantilever had a spring constant of about 5 dyne/cm and its displacement was read out with a optical-fiber interferometer. The microcantilever, which hung from a 2-stage vibration isolation system, oscillated vertically in its lowest flexural mode at a resonant frequency of $\omega_0 \approx 300 \text{ Hz}$. The microcantilever was mounted above an attractor consisting of 5 pairs of alternating $100\mu\text{m} \times 100\mu\text{m} \times 1\text{mm}$ bars of gold and silicon. The attractor was oscillated horizontally underneath the cantilever at about 100 Hz by a bimorph; the amplitude was chosen to effectively resonantly excite the cantilever at the 3rd harmonic of the attractor drive frequency. The geometry was quite complicated; the 3rd har-

monic gravitational force on the cantilever depended sensitively and nonlinearly on the drive amplitude. An electrostatic shield consisting of a $3.0\ \mu\text{m}$ thick silicon nitride plate with 200 nm of gold evaporated onto each side was placed between the cantilever and the attractor. Data were taken with the vertical separations between the cantilever and the attractor as small as $25\ \mu\text{m}$.

4.3.2 Signal-to-noise considerations

The dominant noise source in the Stanford experiment was thermal noise in the cantilever, which was reduced by operating at about 10 K. The Q-factors of the oscillating cantilevers in these measurements were typically about 1200.

4.3.3 Calibration and alignment

The cantilever spring constant k was found in two independent ways that agreed to within 10%: by assuming that when the cantilever was far from the attractor it was in thermal equilibrium with its surroundings, and by calculating k from the measured resonant frequency. The the cantilever was aligned with respect to the attractor using magnetic forces. The cantilever's test mass had a thin nickel film on one of its faces, and the attractor was equipped with a zig-zag conducting path the followed the gold bars. When a current was run through the attractor it placed a force on the cantilever that had half the frequency and phase as the expected gravitational signal but with vastly greater amplitude. This force was used to align the apparatus.

4.3.4 Backgrounds

This experiment was limited by a spurious force about 10 times greater than the thermal detection limit. This force was clearly not fundamental, i.e. related

to the mass distributions on the attractor, because the phase of signal did not behave as expected when the horizontal offset of the attractor oscillation was varied or as the attractor drive amplitude was changed. The most likely source of a spurious force is electrostatics; the cantilever was not metallized so could hold charge and the shield was observed to vibrate by a pm or so. A potential on the cantilever of about 1 V would be sufficient to produce the observed force. Although thin nickel layers were incorporated into the test mass and attractor, the experimenters estimate that magnetic forces from the nickel (as well as from iron impurities in the gold) were too small to explain the observed background force. Vibrational coupling between the attractor and cantilever was minimized because the attractor was moved at right angles to the cantilever's flex.

4.3.5 Results

The experimenters saw a spurious $(8.4 \pm 1.4) \times 10^{-12}$ dyne force at their closest separation of $25\mu\text{m}$. They assigned a 95% confidence upper limit on a Yukawa interaction by computing the minimum α as a function of λ that would correspond to this central value plus 2 error bars. Their constraint, which rules out much of the parameter space expected from moduli-exchange as computed in (98) is shown in Fig. 8

4.4 Casimir force experiments

Early attempts to detect the Casimir force between metal surfaces(151) and dielectric surfaces(152, 153, 154, 155) had relatively large errors. Nonetheless, it was recognized(156, 157, 158) that such measurements provided the tightest constraints on new hypothetical particles with Compton wavelengths less than 0.1

mm. In recent years, three groups have reported measurements of the Casimir force with relative errors of 1% to 5%. Although these experiments are orders of magnitude away from providing tests of the ISL, they do probe length scales from 20 nm to 10 μm , where large effects may occur (see Sec. 2.4.4).

4.4.1 Experimental methods

The first of the recent experiments, performed by Lamoreaux at the University of Washington(136, 159), used a torsion balance to measure the force between a flat quartz plate and a spherical lens with a radius of 12.5 ± 0.3 cm. Both surfaces were coated with 0.5 μm of Cu followed by 0.5 μm of Au. A piezoelectric stack stepped the separation between the plate and lens from 12.3 μm to 0.6 μm , at which point the servo system that held the torsion pendulum angle constant became unstable. The force scale was calibrated to 1% accuracy by measuring the servo response when a 300 mV potential difference was applied between the plate and lens at a large ($\approx 10\mu\text{m}$) separation. The absolute separation between the lens and plate was obtained by applying a potential difference between the two surfaces and fitting the measured force (for distances greater than 2 μm where the Casimir force was small) to the expected $1/d$ dependence, where d is the distance between the plate and lens. After subtracting the $1/d$ component from the force scans, the residual signals were fitted to the expected form for a Casimir force and an agreement to within 5% was found(136, 159).

Mohideen and collaborators at the University of California Riverside reported a series of experiments that used an atomic force microscope (AFM) to measure the Casimir force between a small sphere and a flat plate(137, 160, 161, 162). Their most recent measurement used a 191 μm diameter polystyrene sphere that

was glued to a $320\mu\text{m}$ long AFM cantilever. The cantilever plus sphere and a 1 cm diameter optically polished sapphire disk were coated with 87 nm of Au, with a measured surface roughness of 1.0 ± 0.1 nm. The disk was placed on a piezoelectric tube with the sphere mounted above it, as shown in Fig. 7. The cantilever flex was measured by reflecting laser light from the cantilever onto split photodiodes. The force scale was calibrated electrostatically by applying a ± 3 V potential difference between the sphere and disk at a separation of $3\mu\text{m}$. The force difference between the $+3$ V and -3 V applied potentials was used to determine the residual potential difference between the disk and sphere when their external leads were grounded together: 3 ± 3 mV. The force between the sphere and disk was measured for separations ranging from 400 nm to contact. It was found that the surfaces touched when their average separation was 32.7 ± 0.8 nm. This was attributed to Au crystals protruding from the surfaces. The measured forces were compared to the expected Casimir force for separations from 62 – 350 nm and agreement to within 1% was found(162).

The record for measuring the Casimir force at the closest separation is held by Ederth(163) at the Royal Institute of Technology in Stockholm who measured the force between crossed cylindrical silica disks with diameters of 20 mm. A template-stripping method(164) was used to glue 200 nm layers of Au, with an rms surface roughness of ≤ 0.4 nm, to the silica disks. The Au surfaces were then coated with a 2.1 nm thick layer of hydrocarbon chains to prevent the adsorption of surface contaminants and the cold-welding of the Au surfaces upon contact. One cylindrical surface was attached to a piezoelectric stack and the other to a piezoelectric bimorph deflection sensor that acted as a cantilever spring. The two surfaces were moved toward one another starting at a separation of greater

than $1\mu\text{m}$, where the Casimir force was less than the resolution of the force sensor, and ending at a separation of 20 nm at which point the gradient of the Casimir force was comparable to the stiffness of the bimorph spring, causing the surfaces to jump into contact. The stiffness of the bimorph sensor was calibrated by continuing to move the piezotube another 200 – 300 nm while the surfaces were in contact. The absolute separation between the surfaces was found by fitting the measured force curve to the expected Casimir signal (plus electrostatic background which was found to be negligible) with the absolute separation as a fit parameter. It was found that at contact the surfaces compressed by ≈ 10 nm. The measured force was compared to the expected Casimir force over the range of separations from 20 to 100 nm and an agreement to better than 1% was found.

4.4.2 Signal-to-noise and background considerations

The signal-to-noise ratio for Casimir force measurements as tests of the ISL may be improved by using more sensitive force probes, thicker metallic coatings on the test bodies, and operating at lower temperatures. Nonetheless, the dominant limitation for interpreting the measurements as tests of the ISL come from understanding the Casimir force background to high accuracy. There is a growing literature on the corrections that must be applied to the Casimir force calculated for smooth, perfect conductors at zero temperature (Eqns. 35 & 36). The dominant corrections are for finite temperature, finite conductivity, and surface roughness. Corrections for finite temperature are important for test-body separations greater than $d \approx 1\mu\text{m}$. For the Lamoreaux experiment, the finite temperature corrections at $1\mu\text{m}$ and $6\mu\text{m}$ separations were 2.7% and 174% of the zero-temperature Casimir force, respectively(165). The effects of finite conductivity on the tem-

perature correction were considered by a number of authors(166, 167, 168) and results believed to be accurate to better than 1% were obtained. The correction to the Casimir force for the finite conductivity of the metallic surfaces is of order 10% at $d = 1\mu\text{m}$ and grows with smaller separations. Finite-conductivity corrections using a plasma model for the dielectric function of the metal give the correction as power series in λ_P/d where λ_P is the plasma wavelength of the metal(169, 170, 171). Corrections have also been obtained using optical data for the complex dielectric function(172, 162, 173, 174). Surface roughness of the test bodies contributes a correction to the Casimir force that can be expressed as a power series in h/d where h is a characteristic amplitude of the surface distortion(175, 176, 177, 171). For stochastic distortions, the leading-order surface-roughness correction is $6(h/d)^2$ which is less than 1% of the Casimir force at closest separation in the experiments of Ederth and the Riverside group.

4.4.3 Results

Constraints on Yukawa interactions with ranges between 1 nm and $10\mu\text{m}$, shown in Fig. 8, have been extracted from the Casimir-force measurements of Lamoreaux(165, 148), Ederth(178), and the Riverside group(179, 180, 6, 181). Also shown in Fig. 8 are constraints at even smaller ranges obtained from earlier van der Waals force experiments(182). It should be noted that most of these constraints were obtained by assuming that a Yukawa force could not exceed the difference between the measured force and the predicted Casimir effect. To be rigorous, the raw data should be fitted simultaneously with both Casimir and Yukawa forces, in general, leading to significantly less stringent limits on $|\alpha|$. Deviations from Newtonian gravity in this region that follow a power law (Eq. 3) are constrained more

strongly by the much more sensitive longer-range gravity experiments discussed above(6).

4.5 *Astronomical tests*

A summary of constraints on Yukawa interactions with $\lambda \geq 1$ mm may be found in Figure 2.13 of the 1999 review by Fischbach and Talmadge(13) that we reproduce in part in our Fig. 9. Since the publication of Ref. (13), the constraints for $\lambda \leq 1$ cm have been substantially improved as discussed above. However, the constraints at larger ranges from laboratory, geophysical and astronomical data (see Fig. 9) are essentially unchanged from those given in (13). The astronomical tests provide the tightest constraints on α . These are typically based on Keplerian tests comparing $G(r)M_{\odot}$ values deduced for different planets. However, the tightest constraint comes from lunar-laser-ranging (LLR) studies of the lunar orbit. Because this result may improve significantly in the next few years, we give some details of the measurement here.

The LLR data consist of range measurements from telescopes on Earth to retroreflectors placed on the Moon by US astronauts and an unmanned Soviet lander. The measurements, which began in 1969, now have individual raw range precisions of about 2 cm, and are obtained from single photon returns, one of which is detected for roughly every 100 launched laser pulses(183). The vast majority of the data come from sites in Texas(184) and in southern France(185). The launched laser pulses have full widths at half-maximum of about 100 ps; the return pulses are broadened to about 400 ps because the reflector arrays typically do not point straight back to Earth due to lunar librations. The launch-telescope to lunar-retroreflector ranges have to be corrected for atmospheric delay which is

computed from the local barometric pressure, temperature and humidity. For the Moon straight overhead, the range correction at the Texas site is about 2 m. The dominant uncertainties in converting raw range measurements into separations between the centers of mass of the the Earth and the Moon come from tidal distortions of the Earth and Moon and atmospheric and ocean loading of the Earth. The current model, using the entire world data set, gives an uncertainty of about 0.4 cm in the important orbit parameters.

The most sensitive observable for testing the ISL is the anomalous precession of the lunar orbit. If the Moon were subject only to a central Newtonian $1/r$ potential from the Earth, the lunar orbit would not precess. The orbit does precess due to the Earth’s quadrupole field and perturbations from other solar system bodies, as well as from the small general relativistic geodetic precession and possibly also from a Yukawa interaction; the conventional sources of precession must be accounted for to obtain the anomalous Yukawa precession rate. Ignoring terms of order ε^2 , where the Moon’s eccentricity is $\varepsilon = .0549$, the anomalous Yukawa precession rate $\delta\omega$ is (13)

$$\frac{\delta\omega}{\omega} = \frac{\alpha}{2} \left(\frac{a}{\lambda}\right)^2 e^{-a/\lambda}, \quad (38)$$

where $\omega = 2\pi$ radians/month and a is the mean radius of the Moon’s orbit. The constraint on $\alpha(\lambda)$ is tightest for $\lambda = a/2$ and falls off relatively steeply on either side of $\lambda = a/2$. The current LLR 2σ upper limit on $\delta\omega$ is $270 \mu\text{arc s/y}$; this follows because the observed precession of about 19.2 milliarcseconds/yr agrees with the general relativistic prediction to $(-0.26 \pm 0.70)\%$ where the error is “realistic” rather than “formal” (the error quoted in Ref. (186) should be doubled; J Williams, private communication 2003). We conclude that at 95% confidence $\delta\omega/\omega < 1.6 \times 10^{-11}$; the corresponding LLR constraint is shown in

Fig. 9.

5 CONCLUSIONS

5.1 Summary of experimental results

Because gravity is intimately connected to the geometry of space-time, ISL tests could provide very direct evidence for the existence of extra space dimensions. In addition, ISL tests are sensitive to the exchange of proposed new low-mass bosons. A variety of theoretical considerations, outlined above, hint that new effects may occur at length scales between $10\ \mu\text{m}$ and $1\ \text{mm}$. This, as well as the urge to explore unmapped territory, has motivated the development of new experimental techniques that have produced substantial improvements in constraints upon theories. The overall slope of the experimental constraints shown in Figs. 6, 8 and 9 reflects the rapidly decreasing signal strength of a new interaction as its range decreases. At gravitational strength ($\alpha = 1$ in Fig. 6), the ISL has been verified down to a distance $\lambda = 200\ \mu\text{m}$. At length scales between $20\ \text{nm}$ and $4\ \text{mm}$, many square decades in Yukawa-parameter space have been ruled out. These results have eliminated some specific theoretical scenarios, but many other interesting ideas are still viable as their predicted effects lie somewhat below the current experimental limits.

5.2 Prospects for improvements

5.2.1 Short-range tests of the ISL

To make a gravitational strength ($\alpha = 1$) ISL test at a $20\ \mu\text{m}$ length scale requires an increase in the background-free sensitivity of at least a factor of

10^3 . Fortunately such an increase is possible, although it will require years of development.

The Eöt-Wash group are currently running a new apparatus that features a pendulum/attractor system having 22-fold rotational symmetry with 44 thinner, smaller-diameter holes. The pendulum ring and attractor disk are made from denser materials (copper and molybdenum, respectively). Noise has been improved by a factor of 6. The closest attainable separation has been reduced by a factor of 2 by adding a passive “bounce” mode damper to the fiber suspension system and the thickness of the electrostatic shield has been reduced to $10\mu\text{m}$. Figure 10 shows the spectral density of the torque signal from this apparatus. This instrument should probe Yukawas with $|\alpha| = 1$ for ranges down to $\lambda = 60\mu\text{m}$. In principle, it is possible to use a low-frequency torsion balance in a different mode, one that measures the attraction between two flat plates (JG Gundlach, private communication 2002). This would provide a null test with a sensitivity that scaled as $\lambda^2 e^{-s/\lambda}$ rather than as $\lambda^3 e^{-s/\lambda}$ in the partial-null experiments.

The Colorado group plans to optimize their geometry and to use a Washington-style electrostatic shield to attain closer separations. This could improve their limits between $10\mu\text{m}$ and $50\mu\text{m}$ by at least an order of magnitude. In the long run both groups could run at liquid helium temperatures which will give lower noise, not only from the decreased $k_B T$ factor, but also from the expected increase in the Q-factor of the torsion oscillator. Newman(187) found that the Q-factor of a torsion fiber has two components: one is temperature-independent but amplitude-dependent (this is already negligible in the Eöt-Wash instrument because of the small amplitudes employed) and the other is temperature-dependent

and amplitude-independent.

The microcantilever application exploited by the Stanford group has not yet attained its full potential. Presumably lessons learned in this pioneering experiment will reduce the backgrounds and allow the experimenters to exploit their inherent sensitivity to new very small forces. Because corrections to the idealized Casimir force can be large and depend upon properties of the the test bodies that are troublesome to quantify, it may be difficult to compare Casimir force experiments to theory at an accuracy much better than 1%. The finite-conductivity corrections depend upon the dielectric properties of the actual metallic coating of the test bodies that may differ somewhat from bulk dielectric properties used in the calculation. As the experimental precision improves, parameters associated with the conductivity correction (such as λ_P) may need to be included as adjustable parameters in fitting the measured force versus distance curves. The surface roughness correction should consider distortions over lengths scales larger than are easily accessible by AFM scans and it may necessary to vary the roughness parameters as well. Both corrections scale as inverse powers of the separation, d , as do the corrections for residual electric potential and patch effects. Compounding the problem of multiple corrections with similar distance dependences is the uncertainty in the absolute separation of the test bodies. The Casimir force depends upon $d_0 + d_r$, rather than on d , where d_r is the relative displacement of the test bodies between force measurements (which can be accurately measured) and d_0 is the absolute separation at the origin of the relative scale (which is difficult to determine accurately). Including d_0 as a fit parameter allows other short-distance parameters to vary(163), without affecting the fit at large distances where the fractional error on the force measurements is larger.

It is unlikely that the next few years will see large improvements in Yukawa constraints from Casimir-force experiments.

5.2.2 Long-range tests of the ISL

Because any change in orientation of the Moon's ellipticity grows linearly with time, even with data of constant precision the LLR constraint should improve in proportion as the data span increases (assuming that the modeling of conventional precession sources is not a limiting factor). New LLR projects should improve the raw range precision by an order of magnitude. For example, APOLLO(188) will exploit a 3.5 m telescope at an elevation of 2780 m and sub-arcsecond image quality. This instrument should receive several returned photons per laser shot, giving a data rate about 10^3 times greater than existing facilities. It is expected that more precise data will lead to corresponding improvements in the modeling.

Ranging to other planets, which is needed to probe longer length scales effectively, is currently done using radar (which is limited by the absence of a well-defined "target" on the planet) or else microwave signals transmitted by orbiting spacecraft (which are limited by uncertainties and the finite time-span of the orbits). Furthermore, the accuracy of **microwave** ranges is limited by propagation delay in the interplanetary solar plasma. It is impractical to laser range to passive reflectors on other planets (if they could be placed) because the returned signal falls as $1/r^4$. However, recent developments in active laser transponders, whose sensitivity falls as $1/r^2$, make it practical to place such a device on Mars and ultimately achieve range precisions of a few cm(189). This would yield several interesting new gravitational measurements, including an improved test of the Strong Equivalence Principle(190), which provides one of the best limits on

massless gravitational scalar fields, as well as tests of the ISL that would give interesting constraints on the quasi-localized gravity model of Ref. (125).

ISL tests at scales larger than the solar system typically rely on uncertain astrophysical models. But Will(5) notes that the proposed LISA space-based interferometer could test a pure Yukawa potential at a scale of 5×10^{19} m by studying distortions of the gravitational waveform from an inspiraling pair of $10^6 M_\odot$ compact objects.

5.3 *What if a violation of the $1/r^2$ law were observed?*

Suppose that future experiments revealed a violation of the ISL at short length scales. Of course one would try to tighten the constraints on its range and strength by performing tests using instruments with varying length scales. But a new question immediately arises: is the new physics a geometrical effect of extra dimensions or evidence for exchange of a new boson? This can be decided by testing whether the short-range interaction violates the Equivalence Principle: boson exchange generically does not couple to matter in a universal manner and therefore appears as a “violation” of the Equivalence Principle, while geometrical effects must respect the Principle. Ref. (99) estimated that the Equivalence-Principle “violating” effect from dilaton exchange is $\approx 0.3\%$.

6 ACKNOWLEDGMENTS

This work was supported in part by the National Science Foundation (Grant PHY-997097) and by the Department of Energy. We are grateful to discussions with Z. Chacko, K. Dienes, G. Dvali, S. Dimopoulos, J. Erlich, P. Fox, G. Giudice, J. Gundlach, N. Kaloper, E. Katz, T. Murphy, R. Rattazzi and J. Williams. D.

B. Kaplan collaborated significantly on sections 2.41—2.44. D. Kapner and E. Swanson helped with the figures.

7 NUMBERED LITERATURE CITED

References

1. Riess AG, et al., *Astron. J.* 116:1009 (1998)
2. Perlmutter S, et al. *Astrophys. J.* 517:565 (1999)
3. Erler J and Langacker P, *Phys. Rev. D* 66:010001-98 (2002)
4. Lakes R, *Phys. Rev. Lett.* 80:1826 (1998)
5. Will CM, *Phys. Rev. D* 57:2061 (1998)
6. Fischbach E, Krause DE, Mostepanenko VM, and Novello M, *Phys. Rev. D* 64:075010 (2001)
7. Sucher J and Feinberg G, *Long-range Casimir Forces*, ed. Levin FS and Micha DA, Plenum, New York 1993
8. Drell SD and Huang K, *Phys. Rev.* 91:1527 (1953)
9. Mostepanenko VM and Sokolov IYu, *Sov. J. Nucl. Phys.* 46:685 (1987)
10. Ferrer F and Grifols JA, *Phys. Rev. D* 58:096006 (1998)
11. Fischbach E, *Ann. Phys. (NY)* 247:213 (1996)
12. Adelberger EG, Stubbs CW, Heckel BR and Rogers WF, *Ann. Rev. Nucl. Part. Sci.* 41:269 (1991)
13. Fischbach E and Talmadge CL, *The Search for Non-Newtonian Gravity*, New York: Springer Verlag (1999)

14. Hewitt J and Spiropulu M, *Ann. Rev. Nucl. Part. Sci.* 52:397 (2002) hep-ph/0205106
15. Gell-Mann M, Ramond P and Slansky R, *Rev. Mod. Phys.* 50:721 (1978)
16. Langacker P, *Phys. Rept.* 72:185 (1981)
17. Slansky R, *Phys. Rept.* 79:1 (1981)
18. Kolb EW and Turner MS, *Ann. Rev. Nucl. Part. Sci.* 33:645 (1983)
19. Haber HE and Kane GL, *Phys. Rept.* 117:75 (1985)
20. Wess J and Bagger J, *Supersymmetry And Supergravity*, Princeton, USA Univ. Pr. 1992
21. Dine M, hep-ph/9612389.
22. Dawson S, hep-ph/9712464.
23. Bagger JA, hep-ph/9604232.
24. Lykken JD, hep-th/9612114.
25. Martin SP, hep-ph/9709356.
26. Polonsky N, *Lect. Notes Phys.* M68: 1 (2001) hep-ph/0108236.
27. Poppitz E and Trivedi SP, *Ann. Rev. Nucl. Part. Sci.* 48: 307 (1998) hep-th/9803107.
28. Shadmi Y and Shirman Y, *Rev. Mod. Phys.* 72:25 (2000) hep-th/9907225.
29. Carroll SM, *Living Rev. Rel.* 4: 1 (2001) astro-ph/0004075.
30. Beane SR, *Gen. Rel. Grav.* 29: 945 (1997) hep-ph/9702419.
31. Sundrum R, *J. High Energy Phys.* 9907: 001 (1999) hep-ph/9708329.
32. Bekenstein JD, *Phys. Rev. D* 49: 1912 (1994) gr-qc/9307035.
33. 't Hooft G, gr-qc/9310026.

34. Susskind L, *J. Math. Phys.* 36: 6377 (1995) hep-th/9409089.
35. Bousso R, *Rev. Mod. Phys.* 74: 825 (2002) hep-th/0203101.
36. Aharony O, Gubser SS, Maldacena JM, Ooguri H and Oz Y, *Phys. Rept.* 323: 183 (2000) hep-th/9905111.
37. Schwarz JH, *Phys. Rept.* 89:223 (1982).
38. Green MB, Schwarz JH and Witten E, *Superstring Theory. Vol. 1: Introduction: Superstring Theory. Vol. 2: Loop Amplitudes, Anomalies And Phenomenology* (Cambridge University Press, 1987)
39. Polchinski J, *String Theory. Vol. 1: An Introduction To The Bosonic String, String Theory. Vol. 2: Superstring Theory And Beyond* (Cambridge University Press, 1998)
40. Dienes KR, *Phys. Rept.* 287:447 (1997) hep-th/9602045.
41. Schwarz JH, *Nucl. Phys. Proc. Suppl.* 55B: 1 (1997) hep-th/9607201.
42. Duff MJ, *Int. J. Mod. Phys. A* 11:5623 (1996) hep-th/9608117.
43. Polchinski J, Chaudhuri S and Johnson CV, hep-th/9602052.
44. Polchinski J, *Rev. Mod. Phys.* 68: 1245 (1996) hep-th/9607050.
45. Kiritsis E, hep-th/9709062.
46. Vafa C, hep-th/9702201.
47. Greene BR, Morrison DR and Polchinski J, *Proc. Nat. Acad. Sci.* 95:11039 (1998)
48. Sen A, hep-th/9802051.
49. Taylor WI, hep-th/9801182.
50. Bachas CP, hep-th/9806199.

51. Di Vecchia P and Liccardo A, hep-th/9912161, hep-th/9912275..
52. Johnson CV, hep-th/0007170.
53. Dine M, hep-th/0003175.
54. Arkani-Hamed N, Dimopoulos S, & Dvali GR *Phys. Lett. B* 429:263 (1998)
hep-ph/9803315.
55. Antoniadis I, Arkani-Hamed N, Dimopoulos S and Dvali GR, *Phys. Lett. B*
436: 257 (1998) hep-ph/9804398.
56. Lykken JD, *Phys. Rev. D* 54:3693 (1996) hep-th/9603133.
57. Arkani-Hamed N, Dimopoulos S and March-Russell J, problem,” *Phys. Rev.*
D 63: 064020 (2001) hep-th/9809124.
58. Arkani-Hamed N, Hall LJ, Smith DR and Weiner N, *Phys. Rev. D* 62: 105002
(2000) hep-ph/9912453.
59. Cohen AG and Kaplan DB, *Phys. Lett. B* 470: 52 (1999) hep-th/9910132.
60. Chacko Z, Fox PJ, Nelson AE and Weiner N, *J. High Energy Phys.* 0203:
001 (2002) hep-ph/0106343.
61. Albrecht A, Burgess CP, Ravndal F and Skordis C, *Phys. Rev. D* 65: 123506
(2002) hep-th/0105261.
62. Kaluza T, *Sitzungsber. Preuss. Akad. Wiss. Berlin (Math. Phys.)* K1: 966
(1921).
63. Klein O, *Nature* 118:516 (1926).
64. Klein O, *Z. Phys.* 37:895 (1926) *Surveys High Energy. Phys.* 5: 241 (1986).
65. Giudice GF, Rattazzi R and Wells JD, *Nucl. Phys. B* 544:3 (1999) hep-
ph/9811291.

66. Hewett JL, *Phys. Rev. Lett.* 82:4765 (1999) hep-ph/9811356.
67. Han T, Lykken JD and Zhang RJ, *Phys. Rev. D* 59:105006 (1999) hep-ph/9811350.
68. Mirabelli EA, Perelstein M and Peskin ME, *Phys. Rev. Lett.* 82:2236 (1999) hep-ph/9811337.
69. Hoyle CD et al., *Phys. Rev. Lett.* 86:1418 (2001)
70. Arkani-Hamed N, Dimopoulos S and Dvali GR, and *Phys. Rev. D* 59: 086004 (1999) hep-ph/9807344.
71. Cullen S and Perelstein M, *Phys. Rev. Lett.* 83: 268 (1999) hep-ph/9903422.
72. Barger VD, Han T, Kao C and Zhang RJ, *Phys. Lett. B* 461: 34 (1999) hep-ph/9905474.
73. Hanhart C, Phillips DR, Reddy S and Savage MJ, *Nucl. Phys. B* 595: 335 (2001) nucl-th/0007016.
74. Hanhart C, Pons JA, Phillips DR and Reddy S, *Phys. Lett. B* 509: 1 (2001) astro-ph/0102063.
75. Hall LJ and Smith DR, *Phys. Rev. D* 60: 085008 (1999) hep-ph/9904267.
76. Lykken J and Nandi S, *Phys. Lett. B* 485: 224 (2000) hep-ph/9908505.
77. Damour T, *Phys. Rev. D* 66:010001-148(2002)
78. Kehagias A and Sfetsos K, *Phys. Lett. B* 472: 39 (2000) hep-ph/9905417.
79. Floratos EG and Leontaris GK, *Phys. Lett. B* 465: 95 (1999) hep-ph/9906238.
80. I. Antoniadis, S. Dimopoulos and G. R. Dvali, *Nucl. Phys. B* 516:70 (1998) hep-ph/9710204.

81. Chacko Z and Perazzi E, hep-ph/0210254.
82. Antoniadis I, Benakli K, Laugier A and Maillard T, hep-ph/0211409. This paper quotes $\alpha = 2n/(n + 2)$, due to a factor of 2 error.
83. Lykken JD, prepared for *Theoretical Advanced Study Institute in Elementary Particle Physics (TASI 2000): Flavor Physics for the Millennium, Boulder, Colorado, 4-30 Jun 2000*
84. Landsberg G, hep-ex/0009038
85. Rubakov VA, *Phys. Usp.* 44:871 (2001) *Usp. Fiz. Nauk* 171:913 (2001) hep-ph/0104152.
86. Hewett J and March-Russell J, *Phys. Rev. D* 66: 010001-271 (2002).
87. Uehara Y, *Mod. Phys. Lett. A* 17: 1551 (2002) hep-ph/0203244.
88. Randall L and Sundrum R, *Phys. Rev. Lett.* 83: 3370 (1999) hep-ph/9905221.
89. Goldberger WD and Wise MB, *Phys. Rev. Lett.* 83: 4922 (1999) hep-ph/9907447.
90. Fox PJ, *J. High Energy Phys.* 0102: 022 (2001) hep-ph/0012165.
91. Randall L and Sundrum R, *Phys. Rev. Lett.* 83: 4690 (1999) hep-th/9906064.
92. N. Arkani-Hamed, S. Dimopoulos, G. R. Dvali and N. Kaloper, *Phys. Rev. Lett.* 84:586 (2000) hep-th/9907209.
93. Lykken J and Randall L, *J. High Energy Phys.* 0006: 014 (2000) hep-th/9908076.
94. Dine M, hep-ph/0011376.
95. Moody JE and Wilczek F, *Phys. Rev. D*30:130 (1984)

96. Verlinde E and Verlinde H, *J. High Energy Phys.* 0005:034 (2000) hep-th/9912018.
97. Schmidhuber C, *Nucl. Phys B* 580:140 (2000) hep-th/9912156.
98. Dimopoulos S and Giudice GF, *Phys. Lett. B* 379:105 (1996) hep-ph/9602350.
99. Kaplan DB and Wise MB, *J. High Energy Phys.* 07:67 (2000) hep-ph/0008116.
100. Bars I and Visser M, *Phys. Rev. Lett.* 57:25 (1986)
101. Itoyama H, McLerran LD, Taylor TR and van der Bij JJ, *Nucl. Phys. B* 279:380 (1987)
102. Dvali GR, Gabadadze G and Porrati M, *Mod. Phys. Lett. A* 15: 1717 (2000) hep-ph/0007211.
103. G. R. Dvali, G. Gabadadze and M. Porrati, *Mod. Phys. Lett. A* **15**, 1717 (2000) hep-ph/0007211.
104. Barbieri R and Cecotti S, *Z. Phys. C* 33:255 (1986)
105. Barr SM and Mohapatra RN, *Phys. Rev. Lett.* 57:3129 (1986)
106. Smith GL et al., *Phys. Rev. D* 61:022001-1 (2000)
107. Weinberg S, *Rev. Mod. Phys.* 61: 1 (1989).
108. Carroll SM, Press WH, and Turner EL. *Ann. Rev. Astron. Astrophys.* 30:499 (1992)
109. Weinberg S, astro-ph/0005265.
110. Witten E, hep-ph/0002297.
111. Sundrum R, talk given at Conference on “Frontiers beyond the Standard Model” at Univ. of Minnesota (October, 2002).

112. Rubakov VA and Shaposhnikov ME, Problem,” *Phys. Lett. B* 125: 139 (1983).
113. Gregory R, Rubakov VA and Sibiryakov VM, *Phys. Rev. Lett.* 84: 5928 (2000) hep-th/0002072.
114. Karch A and Randall L, *J. High Energy Physics* 0105: 008 (2001) hep-th/0011156.
115. Dvali GR, Gabadadze G and Porrati M, *Phys. Lett. B* 485: 208 (2000) hep-th/0005016.
116. Dvali GR and Gabadadze G, *Phys. Rev. D* 63: 065007 (2001) hep-th/0008054.
117. Banks T, hep-th/9601151.
118. Horava P, *Phys. Rev. D* 59: 046004 (1999) hep-th/9712130.
119. Cohen AG, Kaplan DB and Nelson AE, *Phys. Rev. Lett.* 82: 4971 (1999) hep-th/9803132.
120. Banks T, II,” hep-th/0007146.
121. Thomas S, *Phys. Rev. Lett.* 89: 081301 (2002).
122. Banks T, hep-ph/0203066.
123. Banks T, hep-th/0206117.
124. Deffayet C, Dvali GR and Gabadadze G, *Phys. Rev. D* 65: 044023 (2002) astro-ph/0105068.
125. Dvali G, Gabadadze G and Shifman M, hep-th/0202174.
126. Dvali G, Gabadadze G and Shifman M, hep-th/0208096.

127. Arkani-Hamed N, Dimopoulos S, Dvali G and Gabadadze G, hep-th/0209227.
128. Dvali GR, Gabadadze G, Kolanovic M and Nitti F, *Phys. Rev. D* 64: 084004 (2001) hep-ph/0102216.
129. Deffayet C, Dvali GR, Gabadadze G and Vainshtein AI, *Phys. Rev. D* 65:044026 (2002) hep-th/0106001.
130. Gruzinov A, astro-ph/0112246.
131. Lue A and Starkman G, astro-ph/0212083.
132. Dvali G, Gruzinov A and Zaldarriaga M, hep-ph/0212069.
133. Mitrofanov VP and Ponomareva OI, *Sov. Phys. JETP* 67:1963 (1988); translation of *Zh. Eksp. Teor. Fiz.* 94: 16 (1988).
134. Hoskins JK, Newman RD, Spero R, and Schultz J, *Phys. Rev. D* 32:3084 (1985)
135. Ederth T, *Phys. Rev. A* 62:062104 (2000)
136. Lamoreaux SK, *Phys. Rev. Lett.* 78:5 (1997)
137. Mohideen U and Roy A, *Phys. Rev. Lett.* 81:4549 (1998)
138. Long JC et al., hep-ph/0210004 (2002)
139. Harris BW, Chen F and Mohideen U, *Phys. Rev. A* 62:052109 (2000)
140. Speake CC, *Class. Quantum Grav.* 13:A291 (1996)
141. Michaelson HB, *J. Appl. Phys.* 48:4729 (1977)
142. Casimir HBG, *Proc. K. Ned. Akad. Wet.* 51:793 (1948)
143. Lifshitz EM, *Sov. Phys. JETP* 2:73 (1956)
144. Gundlach JH & Merkowitz SM, *Phys. Rev. Lett.* 85:2869 (2000)

145. Hoyle CD, *Sub-millimeter Tests of the Gravitational Inverse-Square Law*.
PhD thesis. Univ. Washington (2001)
146. Adelberger EG, *Proc. Second Meeting on CPT and Lorentz Symm.*, ed. V.A.
Kostelecky, World. Sci. p.9 (2002) hep-ex/0202008
147. Saulson PR, *Phys. Rev. D* 42:2437 (1990)
148. Long JC, Chan HW and Price JC, *Nucl. Phys. B* 539:23 (1999)
149. Chiaverini J et al., hep-ph/0209325 (2002)
150. Chiaverini J, *Small force detection using microcantilevers: search for sub-millimeter-range deviations from Newtonian gravity*. PhD thesis. Stanford Univ. (2002)
151. Sparnaay MJ, *Physica (Amsterdam)* 24:751 (1958)
152. Derjaguin BV, Abrikosova II, and Lifshitz EM, *Q. Rev. Chem. Soc.* 10:295 (1956)
153. Tabor D and Winterton RHS, *Proc. R. Soc. London* A312:435 (1969)
154. Israelachvili YN and Tabor D, *Proc. R. Soc. London* A331:19 (1972)
155. Hunklinger S, Geisselmann H, and Arnold W, *Rev. Sci. Instrum.* 43:584 (1972)
156. Kuz'min VA, Tkachev II, and Shaposhnikov ME, *JETP Lett.* 36:59 (1982)
157. Mostepanenko VM and Sokolov IYu, *Phys. Lett. A* 125:405 (1987)
158. Fischbach E, *et al, Metrologia* 29:215 (1992)
159. Lamoreaux SK, *Phys. Rev. Lett* 81:5475 (1998)
160. Roy A, Lin CY, and Mohideen U, *Phys. Rev. D* 60:R111101 (1999)
161. Roy A and Mohideen U, *Phys. Rev. Lett.* 82:4380 (1999)

162. Harris BW, Chen F, and Mohideen U, *Phys. Rev. A* 62:052109 (2000)
163. Ederth T, *Phys. Rev. A* 62:062104 (2000)
164. Wagner P, Hegner M, Guntherodt HJ, and Semenza G, *Langmuir* 11:3867 (1995)
165. Bordag M, Geyer B, Klimchitskaya GL, and Mostepanenko VM, *Phys. Rev. D* 58:075003 (1998)
166. Klimchitskaya GL and Mostepanenko VM, *Phys. Rev. A* 63:062108 (2001)
and references therein
167. Genet C, Lambrecht A, and Reynaud S, *Phys. Rev. A* 62:012110 (2000)
168. Bordag M, Geyer G, Klimchitskaya GL, and Mostepanenko VM, *Phys. Rev. Lett.* 85:503 (2000)
169. Schwinger J, DeRaad LL, and Milton KA, *Ann. Phys. (N.Y.)* 115:1 (1978)
170. Bezerra VB, Klimchitskaya GL, and Romero C, *Mod. Phys. Lett. A* 12:2613 (1997)
171. Klimchitskaya GL, Roy A, Mohideen U, and Mostepanenko VM, *Phys. Rev. A* 60:3487 (1999)
172. Lamoreaux SK, *Phys. Rev A* 59:R3149 (1999)
173. Lambrecht A and Reynaud S, *Eur. Phys. J. D* 8:309 (2000)
174. Bostrom M and Sernelius BoE, *Phys. Rev. A* 61:046101 (2000)
175. Van Bree JLMM, Poulis JA, Verhaar BJ, and Schram K, *Physics (Amsterdam)* 78:187 (1974)
176. Maradudin AA and Mazur P, *Phys. Rev. B* 22:1677 (1980), 23:695 (1981)
177. Klimchitskaya GL and Pavlov YuV, *Int. J. Mod. Phys. A* 11:3723 (1996)

178. Mostepanenko VM and Novello M, *Phys. Rev. D* 63:115003 (2001)
179. Bordag M, Geyer G, Klimchitskaya GL, and Mostepanenko VM, *Phys. Rev. D* 60:055004 (1999)
180. Bordag M, Geyer G, Klimchitskaya GL, and Mostepanenko VM, *Phys. Rev. D* 62:011701R (2000)
181. Mostepanenko VM and Novello M, hep-ph/0008035 v1 (2000)
182. Bordag M, Mostepanenko VM, and Sokolov IYu, *Phys. Lett. A* 187:35 (1994)
183. Williams JG, Newhall XX and Dickey JO, *Phys. Rev. D* 53:6730 (1996)
184. Shelus PJ, *IEEE Trans. Geosci. Remote Sensing* GE-23: 385 (1985)
185. Samain E et al., *Astron. & Astrophys. Suppl. Ser.* 130: 235 (1998)
186. Williams JG, Boggs DH, Dickey JO and Folkner WM, *Proc. 9th Marcel Grossmann Meeting Rome 2002*, p 1797. World Scientific Publ. Co.
187. Bantel MK and Newman RD, *J. Alloys and Compounds* 310:233 (2000)
188. Murphy T et al., http://geodaf.mt.asi.it/GDHTL/news/iwlr/Murphy_et_al_apachepoint.pdf (2000)
189. Degnan JJ, *J. Geodynamics* 34:551 (2002)
190. Anderson JD, Gross M, Nordtvedt K and Turyshev S, *Astrophys. J.* 459:365 (1996)

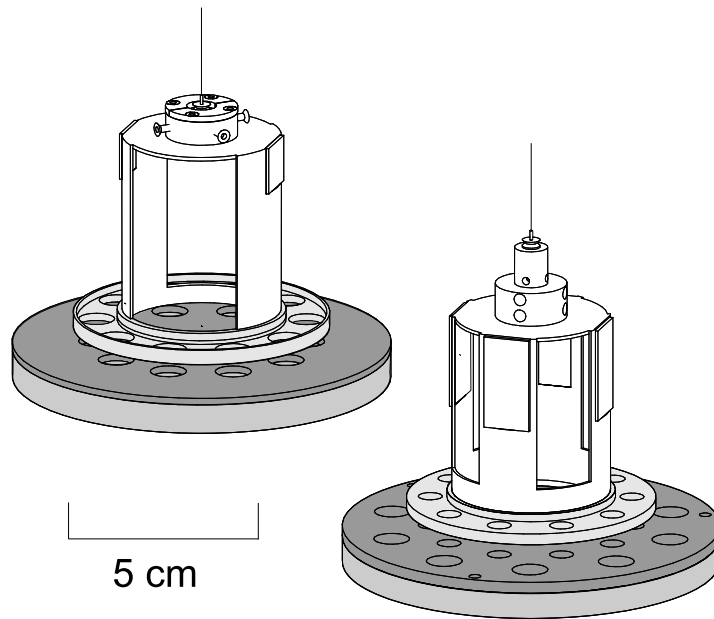


Figure 1: Schematic diagram of the 10-hole pendulums and rotating attractors used in the two experiments of Hoyle et al.(69, 145, 146). The active components are shaded.

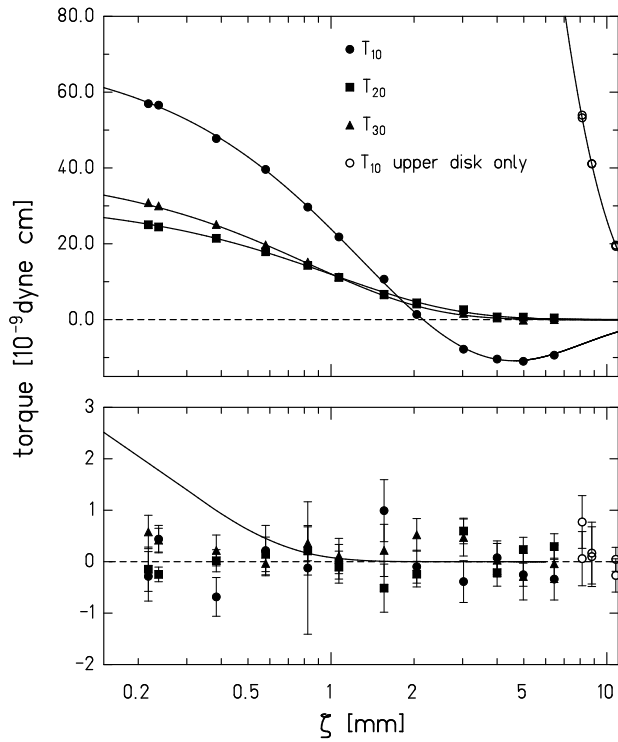


Figure 2: Upper panel: torques measured in the first experiment of Hoyle et al. as a function of pendulum/attractor separation. Open circles are data taken with the lower attractor disk removed and show the effect of uncancelled gravity. Smooth curves show the Newtonian fit. Lower panel: residuals for the Newtonian fit. The solid curve shows the expected residual for a Yukawa force with $\alpha = 3$ and $\lambda = 250 \mu\text{m}$.

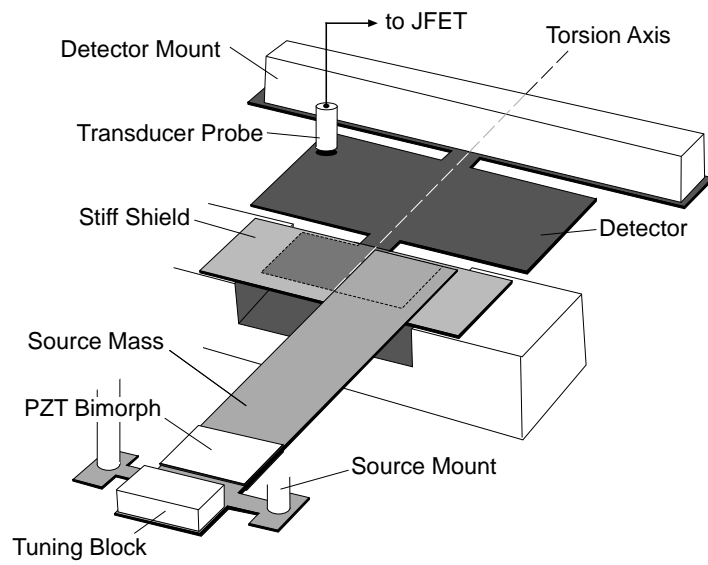


Figure 3: Schematic diagram of the instrument used by Long et al.(138).

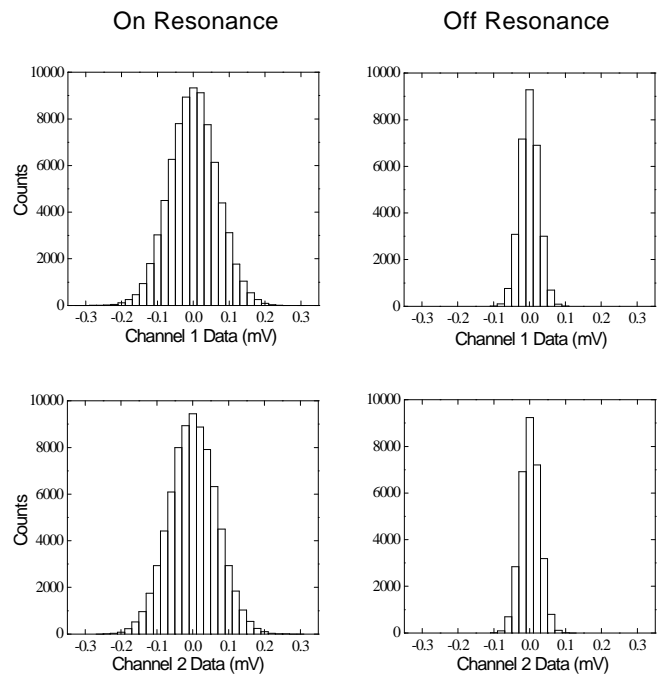


Figure 4: Data from the experiment of Long et al.(138) showing the two quadrature signals from the torsion oscillator.

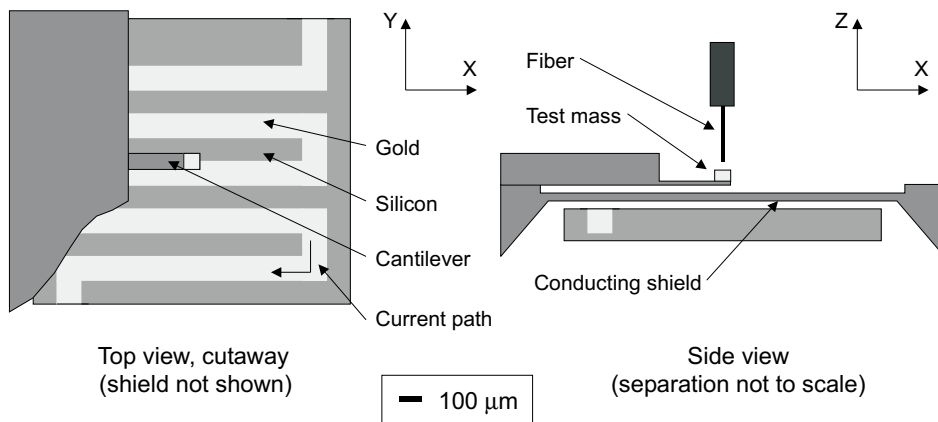


Figure 5: Schematic diagram of the instrument used by Chiaverini et al.(149)

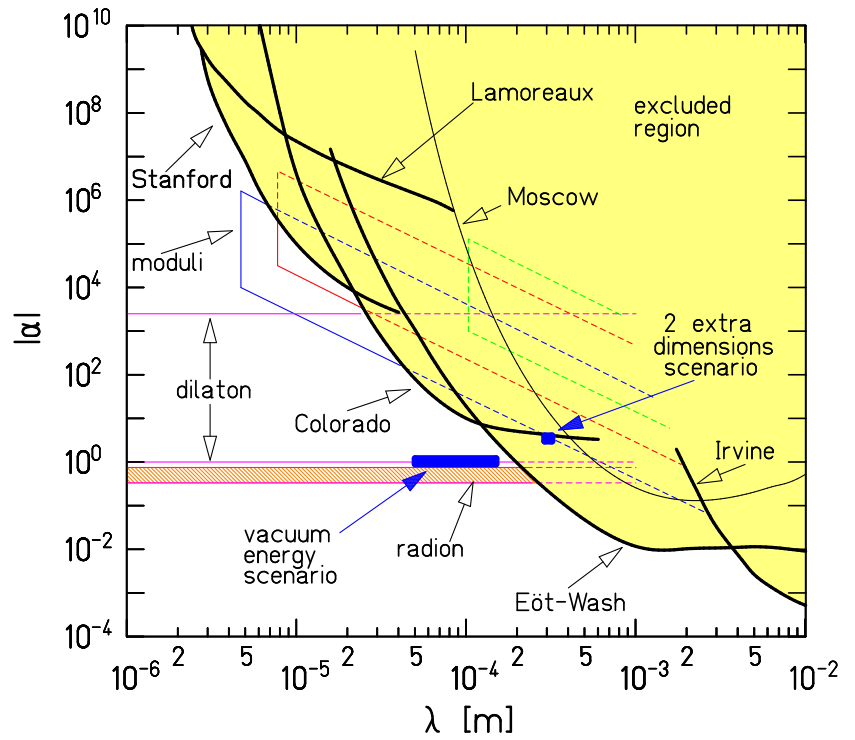


Figure 6: 95% confidence level constraints on ISL-violating Yukawa interactions with $1\mu\text{m} < \lambda < 1\text{ cm}$. The heavy curves give experimental upper limits (the Lamoreaux constraint was computed in Ref. (148)). Theoretical expectations for extra dimensions(54), moduli(98), dilaton(99) and radion(80) are shown as well.

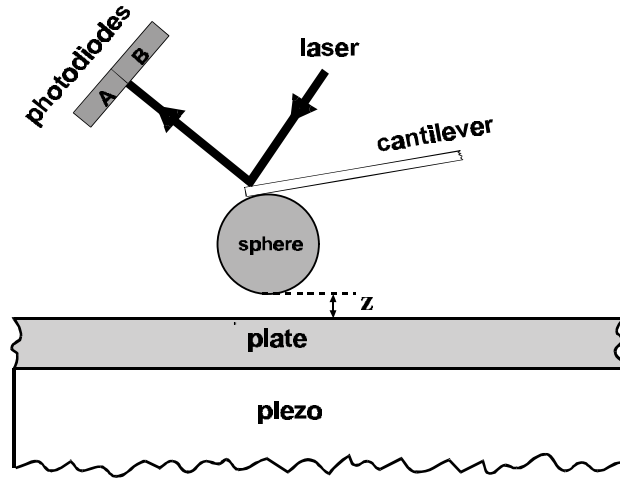


Figure 7: Schematic diagram of the Casimir-force apparatus used in Ref. (162)

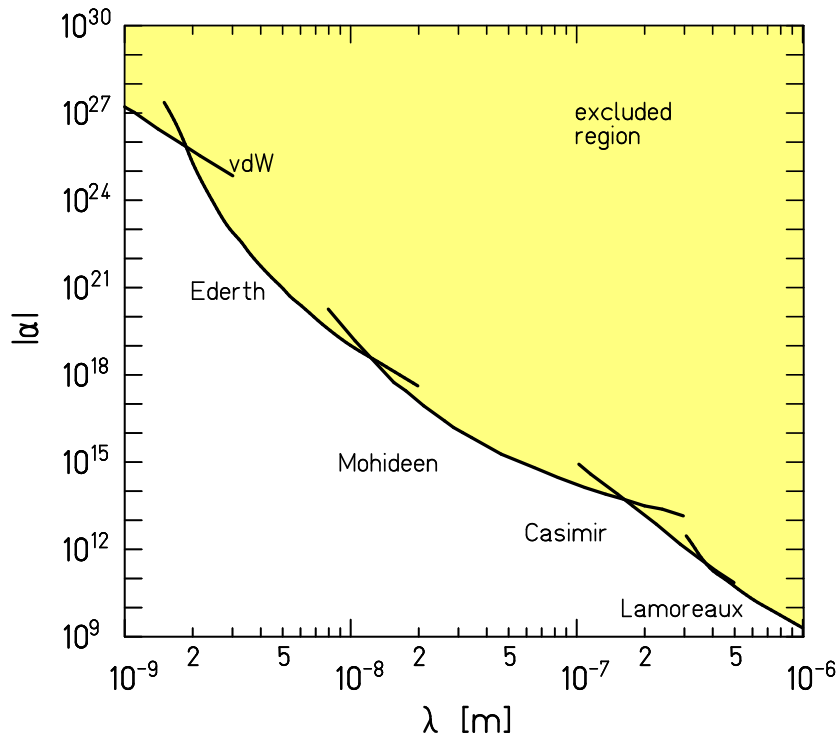


Figure 8: Constraints on ISL-violating Yukawa interactions with $1\text{nm} < \lambda < 1\mu\text{m}$ adapted from Ref. (6). As discussed in the text, these upper limits, extracted from Casimir force measurements, are not as rigorous as those in Figs. 6 & 9.

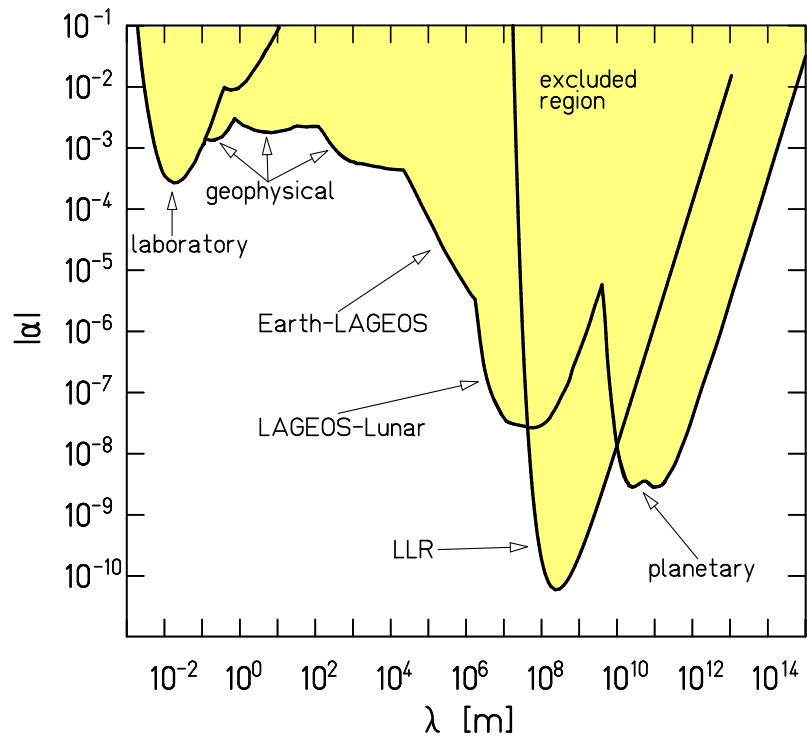


Figure 9: 95% confidence level constraints on ISL-violating Yukawa interactions with $\lambda > 1$ cm. The LLR constraint is based on the anomalous perigee precession; the remaining constraints are based on Keplerian tests. This plot is based on Fig. 2.13 of Ref. (13) and upgraded to include recent LLR results.

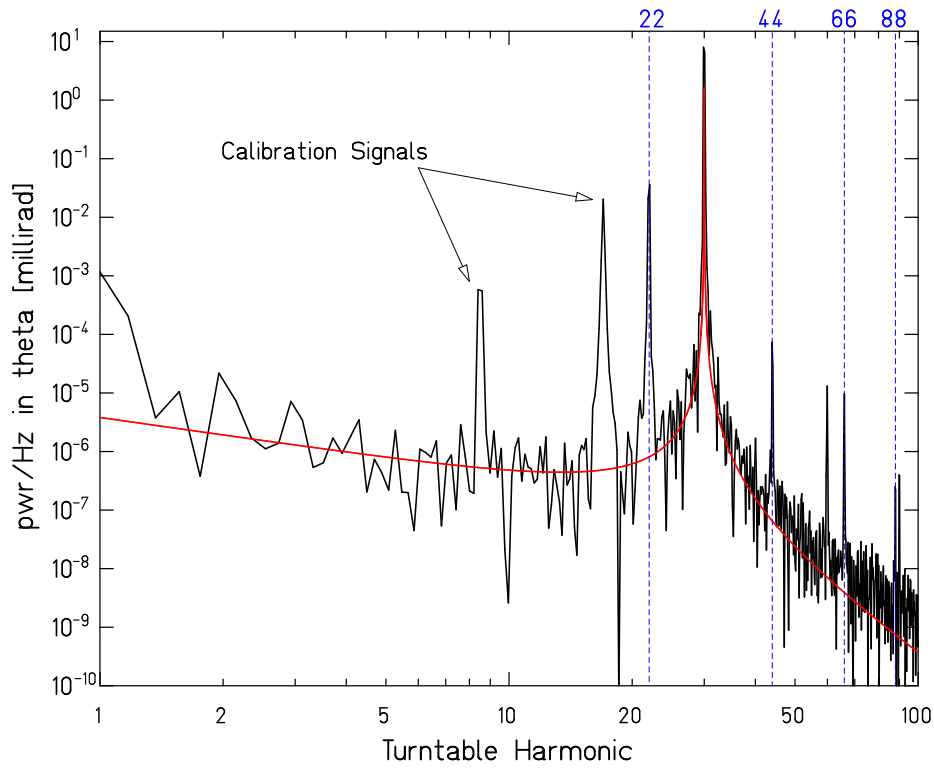


Figure 10: Spectral density of the torque signal in the 22-fold symmetric experiment of the Eöt-Wash group. The peaks at 8.5 and 17ω are gravitational calibrations; the fundamental and first three overtones of the short-range signal are at 22 , 44 , 66 , and 88ω . The smooth curve shows the thermal noise computed using Eq. 33.